CHALMERS
UNIVERSITY OF TECHNOLOGY

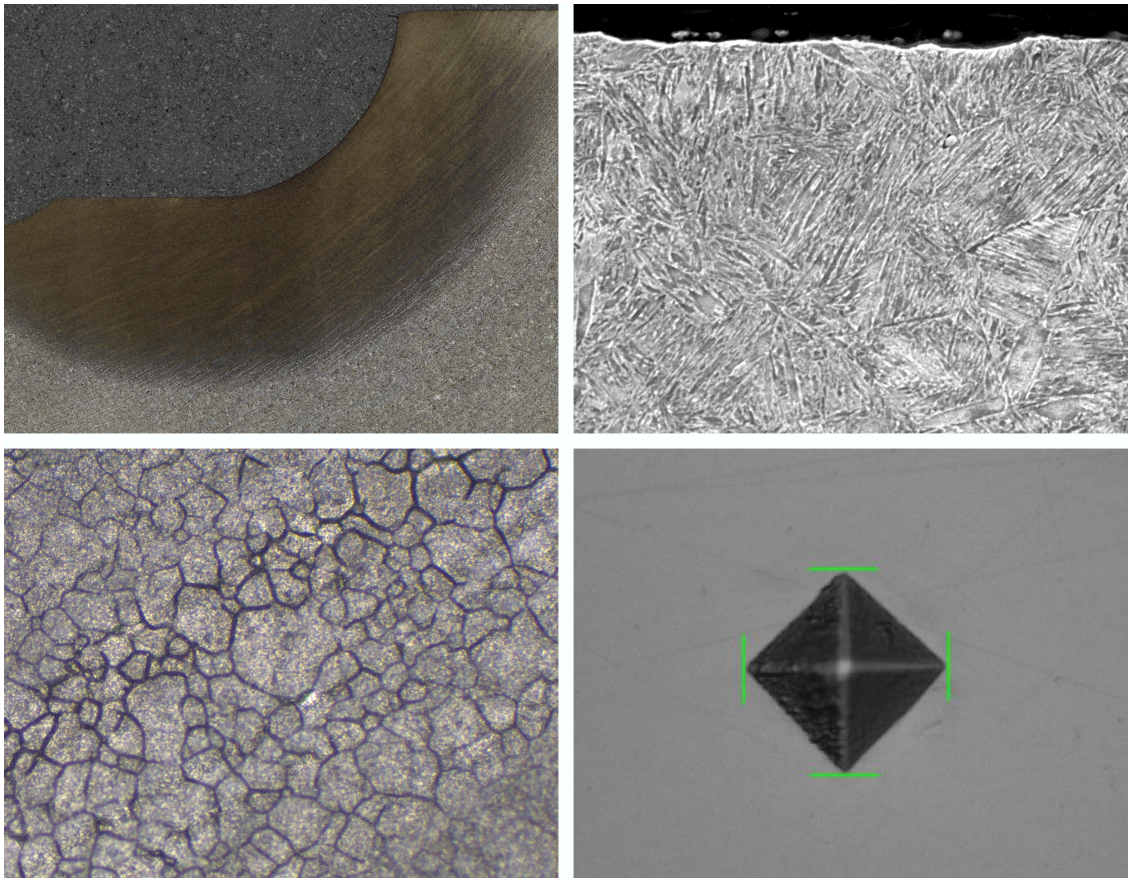

Metallurgical Characterisation Comparing Recycled and Ore-based Steels for Automotive Crankshafts

Master's Thesis in Master Programme Materials Engineering

JOSHUA MICHAEL PAUTZKE

Department of Industrial and Materials Science
CHALMERS UNIVERSITY OF TECHNOLOGY
Gothenburg, Sweden 2020

MASTER'S THESIS 2020

Metallurgical Characterisation Comparing Recycled and Ore-based Steels for Automotive Crankshafts

JOSHUA MICHAEL PAUTZKE

CHALMERS
UNIVERSITY OF TECHNOLOGY

Department of Industrial and Materials Science
Division of Materials and Manufacture
CHALMERS UNIVERSITY OF TECHNOLOGY
Gothenburg, Sweden 2020

Metallurgical Characterisation Comparing Recycled and Ore-based Steels for Automotive Crankshafts
JOSHUA MICHAEL PAUTZKE

Supervisor: Philipp Hoier, Chalmers University of Technology
Examiner: Prof. Uta Klement, Chalmers University of Technology

Master's Thesis 2020
Department of Industrial and Materials Science
Division of Materials and Manufacture
Chalmers University of Technology
SE-412 96 Gothenburg
Telephone +46 31 772 1000

Cover: Upper left: Overview light micrograph of a sidewall sample. Upper right: SEM micrograph of a sidewall surface cross section. Lower left: Light micrograph of a picric acid etched surface revealing prior austenite grain boundaries. Lower right: Light micrograph of a Vickers indent in a surface.

Typeset in LaTeX
Printed by Chalmers Reproservice (Chalmers printing services)
Gothenburg, Sweden 2020

Acknowledgements

I want to thank some people who helped me and gave me advice throughout the whole master thesis project. First of all I want to thank my supervisor at Chalmers, Philipp Hoier, for being available when ever it was needed. He contributed much to this project with his very good ideas, his advice and his unique calmness that was worth more then everything in these times.

Further I would like to thank Uta Klement who was the thesis examiner at Chalmers. Her feedback and help was very useful all the time and she taught me a very important lesson: If you want that people understand what you did, you should have a good story-telling!

I am very grateful to Peter Hammersberg from Chalmers and Ralf Schacherl from University of Stuttgart for organising and supervising my year abroad in Sweden in the frame of the double master degree offered by Chalmers and University of Stuttgart. It has been a great experience that I do not regret and I will never forget it.

I would also like to thank Rasmus Gunnerek for being my opponent during the master thesis seminar and for doing a great correctional reading. The letter also applies to my German friend Alexander von Kiesling who helped me with his skills in English.

Further I want to thank

- Håkan Millqvist for a great a precise work in the workshop,
- Yiming Yao for introducing me into the metallography lab,
- Eric Tam and Dinesh Mallipeddi for introducing me to the residual stress measurement technique and their help whenever it was needed,
- Erika Steyn for introducing me to the optical microscope,
- Lena Magnusson-Åberg, Magnus Persson and Jari Olavison for providing very helpful information and material that was necessary to start with the project,
- Per Lundin for his information and advice on Barkhausen noise analysis,
- the company Bharat Forge Kilsta, especially Niklas Blom, for the received bars and crankshafts.

Lastly, I would like to thank my family, namely my parents Petra Pautzke and Michael Pautzke, my brother Damian and my grandparents Ivana Pohořalá and Jiří Pohořalý. They have been supporting me for a very long time now on every road I decided to go. It is a great thing to have such loving people as a support. All I can say is: Thank you so much!

Joshua Michael Pautzke, Gothenburg, June 2020

Metallurgical Characterisation Comparing Recycled and Ore-based Steels for Automotive Crankshafts

JOSHUA MICHAEL PAUTZKE
Department of Industrial and Materials Science
Chalmers University of Technology

Abstract

Steel crankshafts are a substantial component in internal combustion engines. A critical feature of crankshafts is their bearing surfaces which have to meet tight requirements regarding hardness and compressive residual stresses in order for the component to function properly. The properties of the bearing surfaces are to a large extent determined by a grinding operation which is used as the final step in the manufacturing chain. In practice, it is commonly experienced that there are batch-to-batch material variations which can cause grindability issues leading to unwanted high scrap rates when the surface requirements are not met. These issues are especially pronounced when both steels made from recycled resources and from iron-ore are fed into the production line. The underlying reasons for these grindability variations are largely unknown. The present master thesis project addresses metallurgical differences between a recycled and an iron-ore based steel batch and investigates potential effects on the grindability. Both steel bars (as supplied by steel mills) and the final ground crankshafts are examined. Samples taken from different positions of the crankshaft were investigated using optical and scanning electron microscopy, Vickers hardness testing, Barkhausen noise analysis and XRD residual stress measurements. The results show that there is a significant difference in grain size between the microstructure of the recycled and ore-based initial, as received steel bars. However, metallurgical examination of the unhardened material of the corresponding crankshaft material indicates that these grain size differences have largely been eliminated during the processing steps. When considering the crankshafts, the recycled steel batch is clearly more inhomogeneous but also has a clearly higher hardenability, while the hardness close to the bearing surface only shows insignificant differences. The estimated prior austenite grain sizes and residual stresses seem to differ more within different spots in a material than between recycled and ore-based material.

Keywords: Crankshaft, steel, recycled, ore-based, grindability, microstructure

Contents

List of Figures

List of Tables

List of Abbreviations

Abbreviation	Meaning
Ac_1	Eutectoid temperature
Ac_3	Austenitisation temperature
BN	Barkhausen noise
BNA	Barkhausen noise analysis
BOF	Basic Oxygen Furnace
C	Carbon
CCT	Continuous cooling transformation (diagram)
EAF	Electric Arc Furnace
Fe	Iron
HV	Vickers hardness
NDT	Non-destructive testing
ore	iron-ore based

RS	Residual stress
RT	Room temperature
SEM	Scanning Electron Microscopy
rec	recycled
V6	Pin journal 6
XRD	X-ray diffraction

List of Symbols

Symbol	Meaning	Unit
α_{BN}	Barkhausen noise measuring angle/ position	(°)
BN_{n}	Normalised Barkhausen noise	(1)
d_1	first diagonal Vickers indent	(mm)
d_2	second diagonal Vickers indent	(mm)
d	mean diagonal of d_1 and d_2	(mm)
$d_{\gamma,\mathrm{e}}$	Prior austenite grain size estimate	(µm)
d_{hkl}	Interplanar spacing	(nm)
d_{p}	diameter of position markers	(mm)
F	Applied testing force Vickers	(kgf)
l	Line length (Prior austenite grain size estimation)	(µm)
l_{h}	Distance from hardened sidewall surface	(mm)

N	Number of interceptions per image	(1)
N_l	Number of interceptions per line	(1)
$\sigma_{\mathrm{r},\phi}$	Residual stress in ϕ-direction	(MPa)
ϕ	Rotation angle of residual stress measurement (related to measuring device)	(°)
χ	Tilting angle of residual stress measurement	(°)
θ	Bragg diffraction angle	(°)

1 Introduction

1.1 Grindability Issues in Crankshaft Manufacturing

Since recycling in general enables a more sustainable use of materials, energy and other resources, there is a noticeable strong will and need to use recycled materials in engineering applications. An example of this is the use of recycled steel as a material for automotive crankshafts. Crankshafts as substantial and fast moving components in internal combustion engines need very wear resistant low-friction bearing surfaces. To achieve this, crankshaft bearing surfaces are induction hardened and ground afterwards.

The master thesis project has been proposed in the view of the fact that during the final grinding process, performed by an automotive company, issues may arise which are believed to be caused by batch-to-batch material variations. These issues can include thermal damage (grinding burns) on the ground bearing surfaces. This leads to an undesirable scrap rate and unstable processes. Two different steel producers produce steel bars used for crankshaft manufacturing at the automotive company. One steel company delivers steel bars produced from iron-ore, the other steel company uses scrap steel and recycles it to deliver steel bars. They are referred to as steel bars produced from recycled steel. The steel from both suppliers are the same steel grade. Both recycled and ore-based steel bars are forged to near-net-shaped crankshafts at a forging company. The forged crankshafts are shipped to the automotive company for final processing. The simplified process and supply chain is shown in Figure 1.1. It is supposed that the grinding induced thermal damage is supplier dependent. A possible reason for the grindability issues and the difference in grindability of crankshafts could be compositional and thus microstructural differences in the input material.

There has only been very little research on the effects of batch-to-batch variations on the machinability of crankshafts. Already in 2012 DOVERBO investigated crankshafts made of steels from two different steel suppliers, primarily focusing

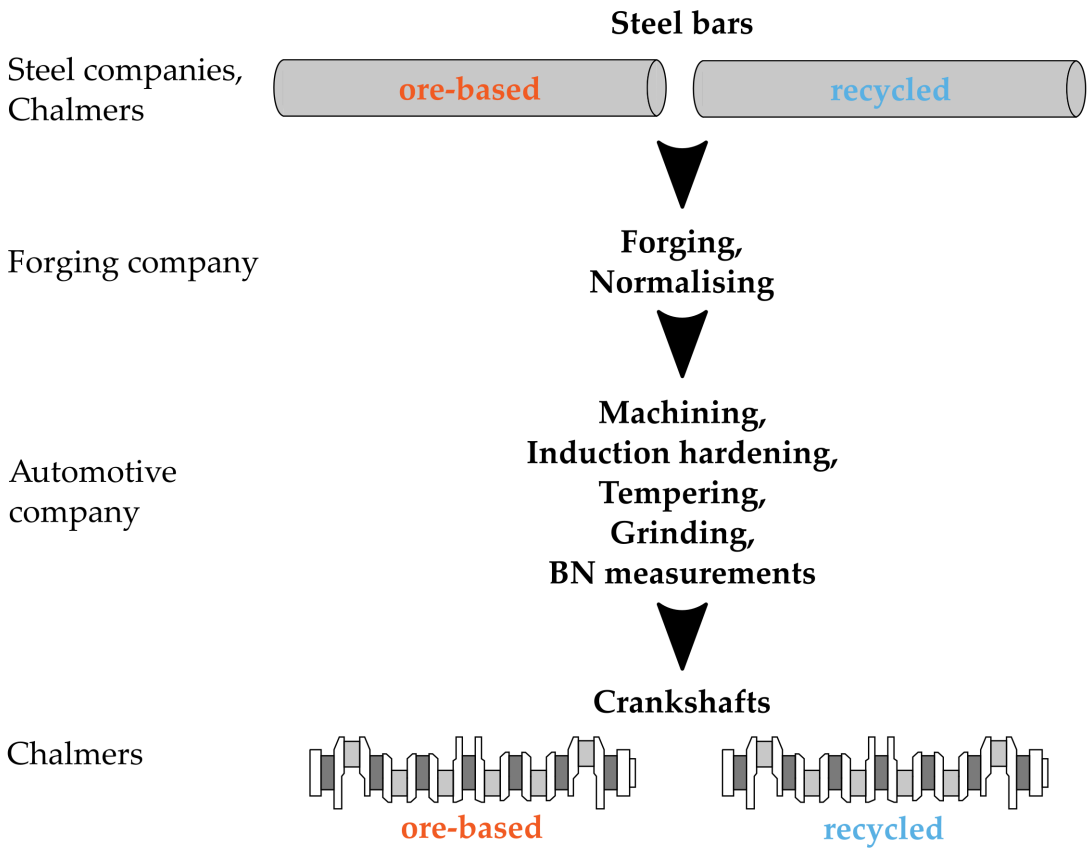

Figure 1.1: Schematic figure of the available material at Chalmers and the manufacturing processes from steel bar to crankshaft.

on the material properties and their correlation with grinding effects. It could be shown that while the composition and microstructure of both steels was similar, they differed a little in terms of impurity distribution [1]. Later, MACHADO investigated the tool wear in crankshaft turning of five different batches observing that non-metallic inclusions, their type, amount and size distribution play a major role for the wear of turning tools and that it can be responsible for the inconsistent behaviour of the different batches during turning [2]. However, none of these works focuses on the crankshafts, their manufacturing and the impact the manufacturing has on the final microstructure.

1.2 Aims

The aims of the thesis project are to investigate the microstructure of both recycled and iron-ore based steel bars to elaborate possible differences in the materials' initial microstructures. Further, the microstructure of both recycled and iron-ore

based steel crankshafts at the ground and grindability critical sidewall surfaces are to be investigated to elaborate possible differences in the material's final microstructure. To obtain an insight into mechanical properties hardness is to be measured. Using data from non-destructive testing (NDT) methods like Barkhausen noise analysis (BNA) and residual stress (RS) measurements using X-ray diffraction (XRD) are supposed to serve as criteria for grindability. By achieving these aims the research question should be able to be answered.

The research question is, in which manner and to what extent the recycled and ore-based steel bars and crankshafts are dissimilar in microstructure and hardness and to how these differences might affect grindability and grinding defects like grinding burns.

1.3 Limitations

The microstructure of a material strongly depends on the manufacturing processes the material is exposed to and can statistically variate within a part. The investigated crankshafts have a very high volume. In addition, metallographic examinations focus on small sites and are very time-consuming. The conclusions of this thesis project are of course drawn from the results obtained from measurements at the investigated sites, which represent a minor part of the whole component. This thesis project focuses primarily on crankshafts sidewalls.

2 Background

This chapter gives necessary background information on the crankshafts' material and the material's characteristics. Later, information on the crankshaft design and production as well as non-destructive testing methods related to the master thesis project are given.

2.1 The Material

2.1.1 Classification

The investigated crankshafts are made of a material that can be classified as low-carbon microalloyed steel. With a carbon content of around 0.45 wt% it is a hypoeutectiod steel with a ferritic-pearlititc microstructure in the near-equilibrium microstructure that is obtained under slow cooling. The following section gives an insight on the microstructure of hypoeutectoid steels, the present microconstitutents and phases.

2.1.2 Microstructure, Microconstituents and Phases

The appearance and the properties of a material's microstructure at room temperature is strongly dependent on the material's thermal and mechanical history, e.g. heat treatments, cooling rates and deformation due to manufacturing. For steels this dependence is shown in the phase diagram (see Figure 2.1 a)) and the continuous cooling transformation (CCT) diagram (see Figure 2.1 b)). While the phase diagram shows the phases that form under near-equilibrium thermodynamic conditions, the CCT diagram shows the influence of the cooling rate: Under these non-equilibrium thermodynamic conditions, other phases form than in the near-equilibrium case [3].

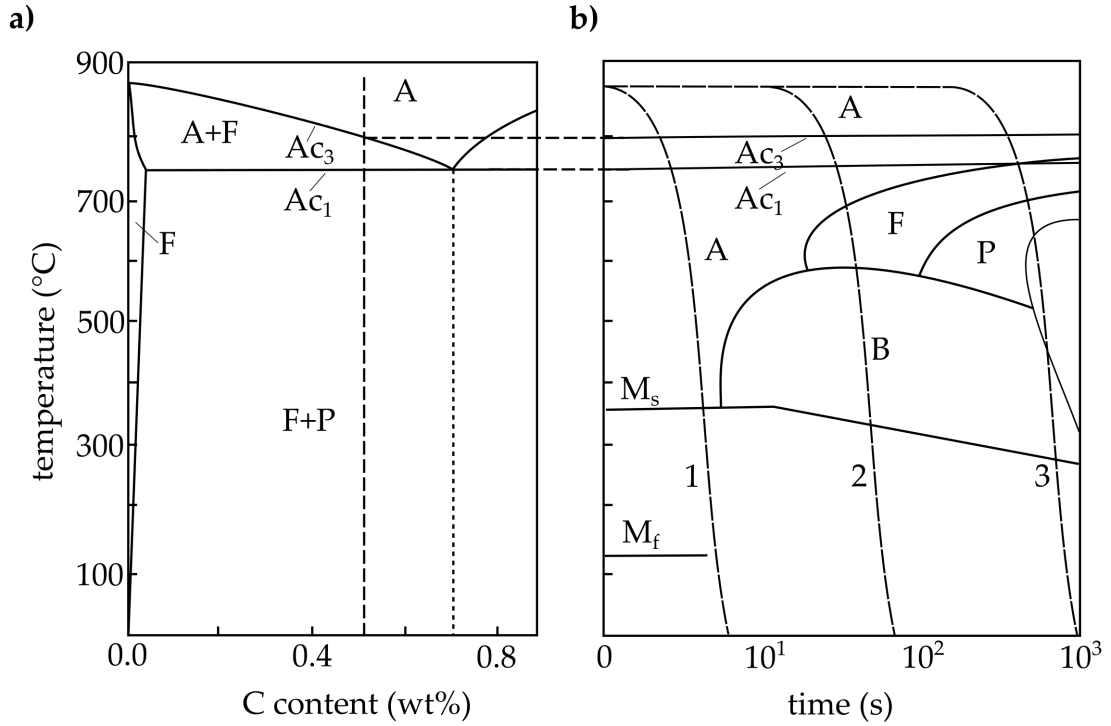

Figure 2.1: Schematic qualitative drawing of **a)** the iron-carbon phase diagram and **b)** the corresponding continuous cooling transformation (CCT) diagram (modified from [3]). F: Ferrite. P: Pearlite. A: Austenite. B: Bainite. M_s: Martensite start temperature. M_f: Martensite finish temperature. Ac_1: Temperature of ferrite/-pearlite to ferrite/austenite transformation. Ac_3: Temperature of ferrite/austenite to austenite transformation. 1: Continuous cooling curve for high cooling rate. 2: Continuous cooling curve for medium cooling rate. 3: Continuous cooling curve for low cooling rate.

2.1.2.1 Near-equilibrium Microstructure in Hypoeutectiod Steels

A near-equilibrium microstructure in hypoeutectoid steels is obtained when cooling rates from above Ac_3 are very low, as e.g. in air cooling. The phase diagram in Figure 2.1 a) shows the present phases in dependence of temperature and carbon content. For the investigated steel, the vertical dashed line can be assumed as the line of constant carbon content and changing temperature. Above Ac_3, only austenite is present. Austenite is also referred to as γ-iron and has a face-centered cubic (fcc) crystal structure [4]. Furthermore, the carbon solubility of austenite is relatively high compared to other phases. In this phase region most of the heat treatment processes are done. These are described in the section 2.2.3. When the system's temperature sinks below Ac_3 but is still above Ac_1, the system enters the two-phase region. Here, ferrite forms out of some austenite grains, while the other austenite grains remain. Ferrite (α-iron) has body-centered cubic (bcc) crystal structure and a very low carbon solubility. It is almost pure iron or can at least be considered as such. Ferrite is ductile, soft and has a very low strength [4]. Below Ac_1 the remaining austenite grains decompose in an eutectoid reaction to lamellar ferrite and cementite (iron carbide, Fe_3C). The areas with lamellar ferrite and cementite are refereed to as pearlite.

2.1.2.2 Non-equilibrium Microstructure in Hypoeutectiod Steels

A non-equilibrium microstructure in hypoeutectiod steels is obtained when cooling rates from Ac_3 are very high as for curve 1, indicated in the CCT diagram in Figure 2.1 b). Instead of the previously described transformations, austenite remains the only phase until the martensite start temperature M_s is crossed.

Because of the very high cooling rates, carbon atoms cannot diffuse out of the austenite that has a decreasing solubility for carbon with reducing temperature. A supersaturated solution is created and carbon diffusion out of the austenite grains is suppressed [5]. As a result, the fcc austenite transforms into body-centered tetragonal (bct) martensite leading to a very hard and brittle phase in a diffusionless process. The transformation is accompanied by a slight volume increase, leading to compressive residual stresses in martensitic surface layers [3].

However, not necessarily the whole austenite transforms into martensite below the martensite finish temperature M_f. A certain amount remains austenitic and is termed *retained austenite*. For the investigated steel with about 0.45 wt% carbon,

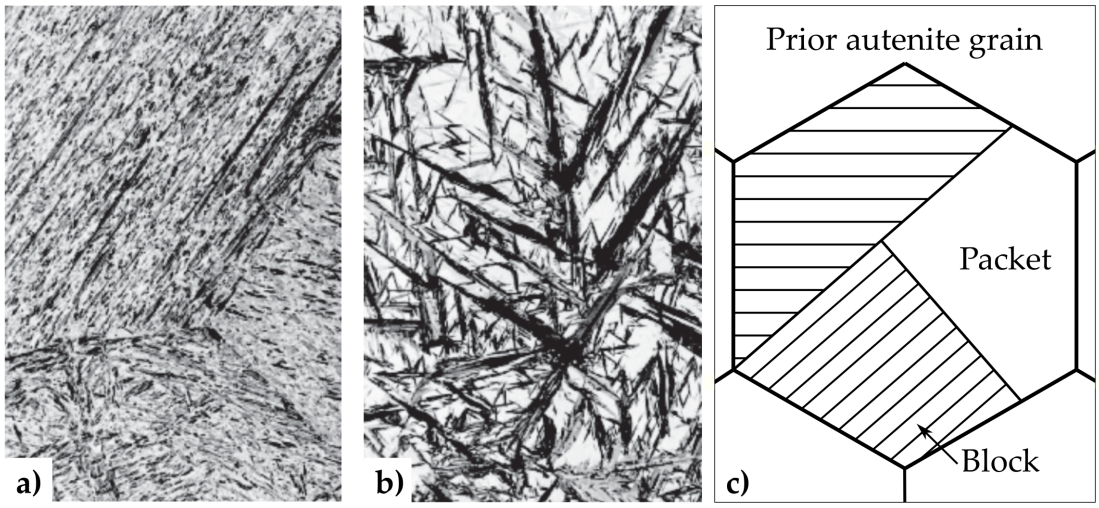

Figure 2.2: a) Lath martensite [3]. **b)** Plate martensite [3]. Images a) and b) reproduced with permission from *Springer Nature*[1]. **c)** Microstructural hierarchy of lath martensite structure (modified from [8]).

a retained austenite content of below 5% of the whole volume can be expected, while the martensite is supposed to consist of 80% lath martensite [5]. Typically, in steels with carbon contents between 0.4 and 0.8 wt% a mixture of lath and plate martensite is present [3]. The micrographs in Figure 2.2 a) and b) show the appearance of both lath and plate martensite. The sudden martensite formation takes place within the austenite grains. In a prior austenite grain many differently oriented packets of similarly oriented lath martensite can form (see Figure 2.2 c)). The prior austenite grain size directly affects the packet size of lath martensite and the smaller the packets, the stronger the material [6].

Tempering at elevated temperatures reduces the hardness of martensite due to the thermally activated rearrangement of dislocations within the martensite laths and the accompanied reduction of dislocation density [5]. Furthermore, compressive residual stresses are relieved [3] while the toughness is being increased [7].

2.1.3 Hardenability and Hardness

Hardness is a mechanical property that is generally defined as a materials "resistance to permanent indentation" at its surface [9]. Hardness is a commonly tested property, but it is not fundamental since the resistance measured during

[1]Reproduced with permission from *Springer Nature*: Ferrous Materials - Steel and Cast Iron by Hans Berns and Werner Theisen, Springer-Verlag Berlin Heidelberg 2008

a hardness test is dependent on both the indenter shape and load applied [9]. Therefore, many different hardness tests with different indenter shapes have been developed e.g. Brinell, Knoop or Vickers hardness testing.

Hardenability can be defined in many different ways. A short definition is, that hardenability is the "susceptibility to hardening by rapid cooling" [10]. According to SIEBERT et al. [11] hardenability is "the capacity of a steel to transform partially or completely from austenite to some percentage of martensite at a given depth when cooled under some given conditions". This latter definition is precise and open enough to compare steels' hardenabilities. With this definition, both a steel with a high maximum hardness but a short hardening depth and a deeper hardened steel with a lower maximum hardness can be considered as steels with good hardenability. The hardenability assessment depends on the aspects that are considered important, usually hardness or hardening depth.

When cooling rate and quenchant are kept constant, hardenability is mostly affected by austenite grain size and chemical composition. In general, hardenability increases with austenite grain size, since there are less grain boundaries where ferrite and pearlite could nucleate. Alloying a steel with elements that slow down the formation of ferrite and pearlite increase the steels hardenability. [5]

2.1.4 Residual Stresses in Surface-hardened and Ground Steels

Residual stresses are those that remain within a material when no external loads are applied [12]. They are generally divided in three types, depending on how large their distance of variation is. Type I residual stresses, also macro residual stresses, describe the stress variation in a range far over the grain size, while type II residual stresses vary over the grain scale and type III residual stresses over the atomic scale [13].

The origin of residual stresses can be various: They can be induced by mechanical (plastic deformation), thermal (heat/cold, thermal gradients) and chemical (reactions, phase transformations) influences [14]. This clarifies that almost every manufacturing process or heat treatment is accompanied by the generation of residual stresses in the material. When considering surface-hardened and ground steels, two main effects have to be mentioned: In the hardening process the rapid cooling of austenitised steel leads to the formation of martensite. This is accompanied by a crystal structure change and a volume expansion leading to strains

and thus to compressive stresses in the martensitic microstructure [15]. These are highly desired since they increase fatigue strength and wear resistance [12].

On the other hand there is the grinding operation performed on hardened surfaces that is reducing the compressive residual stresses created in the hardening process. These decrease the fatigue strength and even the corrosion resistance. This contributes to a lower service life. [12] If done properly, grinding can maintain compressive residual stresses in the surface while attaining precise geometrical dimensions on the work piece.

2.2 Crankshafts

2.2.1 Purpose and Relevance

Crankshafts are often referred to as the "heart of the engine". It is indeed a basic part in nearly every combustion engine used nowadays. Within internal combustion engines the crankshaft converts the linear motion of pistons along the cylinder into rotational motion of its own axis [7]. Crankshafts are commonly found in the internal combustion engines of automotive vehicles like cars and trucks. The crankshafts investigated in this thesis are steel crankshafts for truck engines.

2.2.2 Design

The shape of the investigated truck crankshafts can be described as a rod with an irregular shape. Figure 2.3 a) shows a schematic image of a crankshaft labelling the different functional parts. Between the front and rear end the crankshaft has many bearing surfaces which belong to either main or pin journals. In the mounted state, the main journals are attached to the engine block while the pistons' connecting rods are attached to the pin journals [7]. Main and pin journals are arranged in an alternating manner, connected by parts called web. The main and pin journals bearing surface can be divided into three relevant surfaces: the diameter surface, the radius surface and the sidewall surface. To reduce friction these bearing surfaces are ground to have a low roughness and induction hardened to withstand wear and tear.

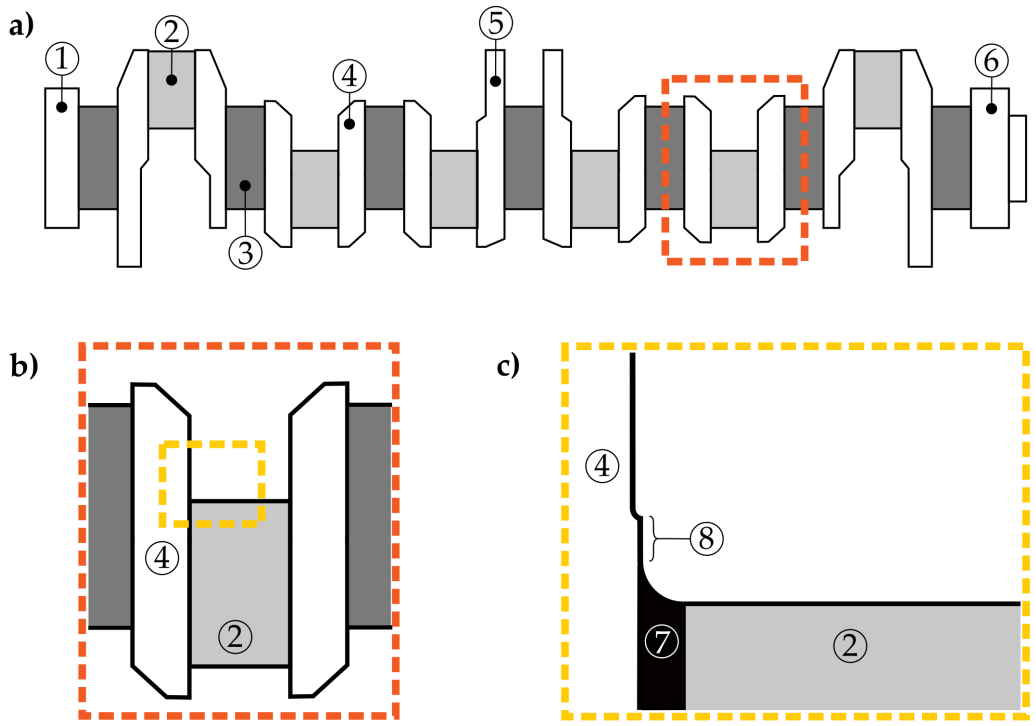

Figure 2.3: Schematic crankshaft design. **a)** whole crankshaft, **b)** crankshaft details at pin journal, **c)** pin journal details. 1: Rear end, 2: Pin journal, 3: Main journal, 4: Web, 5: Counterweight, 6: Front end, 7: Radius, 8: Sidewall.

2.2.3 Manufacturing

Crankshafts are manufactured using three different methods. Manufacturing via machining from a solid metal block is only used for small series that are used for prototypes or in motor racing applications. Manufacturing crankshafts via casting is the most cost-efficient method, but is not applied for e.g. truck crankshafts where the expected loads demand a material with high strength. In that case, crankshafts are manufactured via forging.[7]

In the following, a closer look is taken on the processing steps undertaken in crankshaft forging.

2.2.3.1 Primary Steelmaking

The steel used for the manufacturing of forged crankshafts can be based on iron-ore or recycled steel. GUPTA refers to *primary metals* if they are generated from naturally occuring resources like ores and *secondary metals* if the material is obtained via recycling of scrap [16]. Depending on the origin of the steel, i.e. if the

steel is iron-ore based (primary) or recycled (secondary), the *primary steelmaking* differs.

Primary steelmaking is the process in which crude steel is obtained. Many processes are being summarized under this term, but the most known and to be mentioned processes are the *Basic Oxygen Furnace* (BOF) process and the *Electric Arc Furnace* (EAF) process.

The BOF process, also known as Linz–Donawitz process, is used for producing iron-ore based steel. It requires primarily liquid pig iron, which is provided by the blast furnace in the ironmaking process, iron ore, fluxes and a metallic iron source which can be directly reduced iron or steel scrap. By blowing oxygen on or into the liquid pig iron, carbon gets oxidised and released as carbon dioxide. This reduces the high carbon content of approximately 4-4.5% in the pig iron which then is considered crude steel. It is necessary to mention, that pretreatment of the pig iron is possibly done before the BOF process and that there is more processing steps and reactions going on in the BOF than mentioned here. A closer view on the details of the BOF process is given by MILLER et al.[17]

The EAF process is applied for the production of recycled steel from steel scrap. It relies solely on steel scrap [6], but the addition of clean iron units like direct reduced iron or hot briquetted iron is common. To melt the steel scrap in the EAF, high voltage is applied between the graphite electrodes and the anode. This creates a electric arc with a temperature above the melting temperature. Further details of the EAF process are described by JONES et al.[18]

2.2.3.2 Secondary Steelmaking

Usually, the steel resulting from primary steel making is being refined in processes that are referred to as *ladle steelmaking* or *secondary steelmaking*. The aim of secondary steelmaking is to get all the alloying elements in the steel to the desired precise levels set in the corresponding grade specification. This is accomplished by operations such as deoxidation, degassing, desulfurisation and alloying. GHOSH describes the different aspects and processes of the secondary steelmaking in *Secondary Steelmaking: Principles and Applications*. [19]

2.2.3.3 Continuous Casting

When the steel's composition is set, the liquid steel melt is first cast into an intermediate vessel, the so called tundish. From the tundish, the liquid steel is tapped into a water-cooled mold, where it solidifies. Pinch rolls positioned straight after the mold draw the now solidified steel through the mold with constant velocity [9]. Like this, a continuous steel bar of round or rectangular shaped face is cast. The continuous bar is cut into sections in the last step of the continuous casting process [7].

2.2.3.4 Hot-Rolling

The continuous bar sections created at the end of the continuous casting process are heated to about 1200 °C in a downstream walking beam furnace to then enter a rolling line. After several rolling stages and a cutting step, the bars reach their final and specified dimensions. This is the last step of the bar manufacturing, but usually the material is being inspected before shipping. [7]

Rolling at elevated temperatures has an intense effect on the steel's microstructure: The high temperatures activate the slip-systems in the austenite grains. Thus, subsequent plastic deformation at high temperatures leads to a high dislocation density in the plastically deformed and elongated austenite grains after rolling. The introduced high strain energy in the material and the high temperature then drives the nucleation and growth of new small equiaxed austenite grains, so called recrystallisation. The elongated and large grains are replaced by smaller grains and transform to ferrite and pearlite upon cooling to room temperature. [3], [6]

In rolled steels so called banding can occur. Banding occurs due to dendritic segregation and subsequent rolling. During the solidification in processes like the continuous casting, dendritic grains grow from the cast pieces outer boundaries accompanied with segregation which leads to different chemical compositions in the firstly crystallised dendrites and the later solidified liquid. The segregates are later elongated and oriented due to the rolling process. According to KRAUSS banding "is the microstructural condition manifested by alternating bands of quite different microstructures aligned parallel to the rolling direction of steel products"[6]. Banding can be visible after etching of surfaces through aligned inclusions, distribution of phases or small etching differences due to different chemical composition.[6]

2.2.3.5 Hot-Forging

Forging is the manufacturing step where the initial cylindrical steel bar is formed to the rough crankshaft shape. However, this can not be achieved in one single forging step but is performed in a number of sequential steps with special dies. This approach minimises the machining after forging. [7]

Before forging, the steel bar is induction heated up to between 1100 °C and 1300 °C. The steel bar then has a fully austenitic microstructure due to the high temperatures (see Figure 2.4). Forging at higher temperatures reduces the forces needed to plastically deform the material. In the forging process the steel bar is placed between two dies which are pressed against each other (see Figure 2.5). The material deforms plastically and fills the voids in the dies by "flowing" into them (see Figure 2.5) [9]. Six-cylinder crankshafts may undergo an additional step where a special machine, integrated in the forging line, twists two pins by 60° [7].

After all the particular forging steps, the forged crankshaft cools down under controlled conditions. The austenitic microstructure transforms back into a ferritic-pearlitic microstructure as shown in Figure 2.4. A grain-flow pattern remains.

2.2.3.6 Normalising

Normalising is a heat treatment that is performed in order to obtain a fine and uniform (homogeneous) grain size in ferritic-pearlitic steels [3]. It reduces residual stresses and improves machinability [9]. It is often applied to hot-forged carbon steels, especially when bars are forged to complex shapes at high temperatures in the austentite phase field. The temperature during forging of complex shapes can be well above the grain-coarsening temperature. Due to that, some grain coarsening may occur during handling of the hot crankshafts between the particular forging steps or in the initial phase of cooling down. As a result of that the austenitic and the subsequent ferritic-pearlitic microstructure is coarse. Because of different degrees of deformation in the complex shaped forging, the grain size may not only be coarse, but even quite different depending on the position in the forging and its deformation during forging [6]. To normalise a forging, it is heated up to approximately 100 °C above austenitisation temperature Ac_3 for a short time and subsequently cooled in static air [5], [9]. Figure 2.4 shows the normalising process in a qualitative time-temperature diagram.

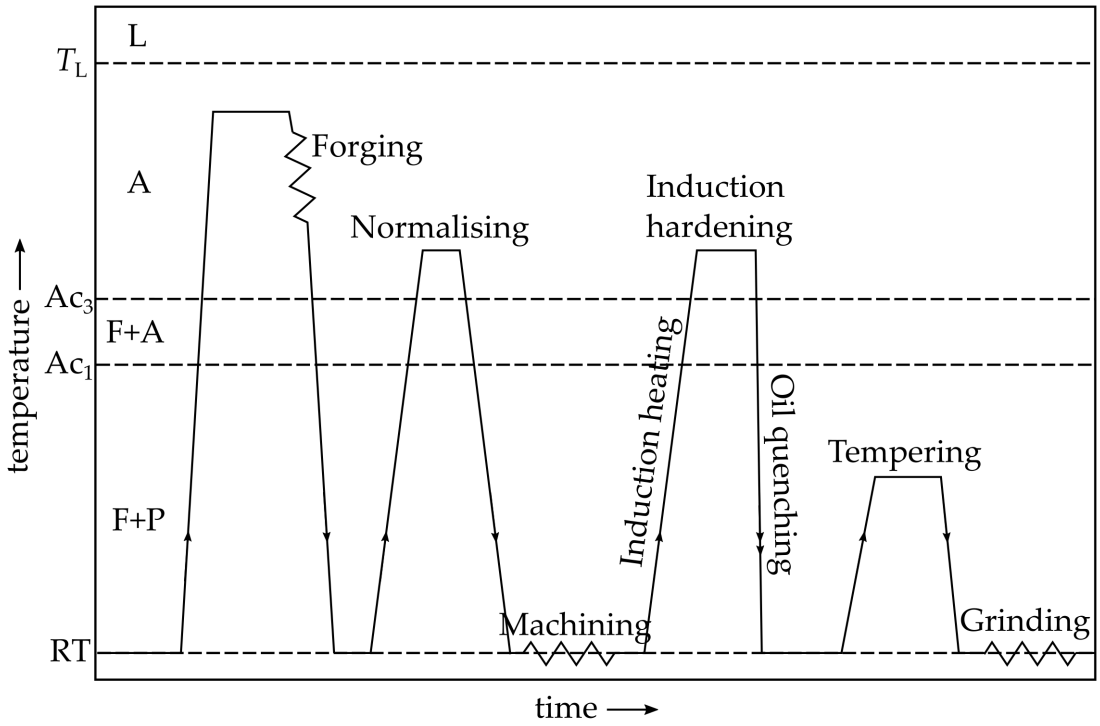

Figure 2.4: Schematic qualitative drawing of the crankshaft manufacturing processes with respect to process temperature and chronology. L: Liquid iron phase field. A: Austenite phase field. F+A: Ferrite/austenite phase field. F+P: Ferrite/-pearlite phase field.

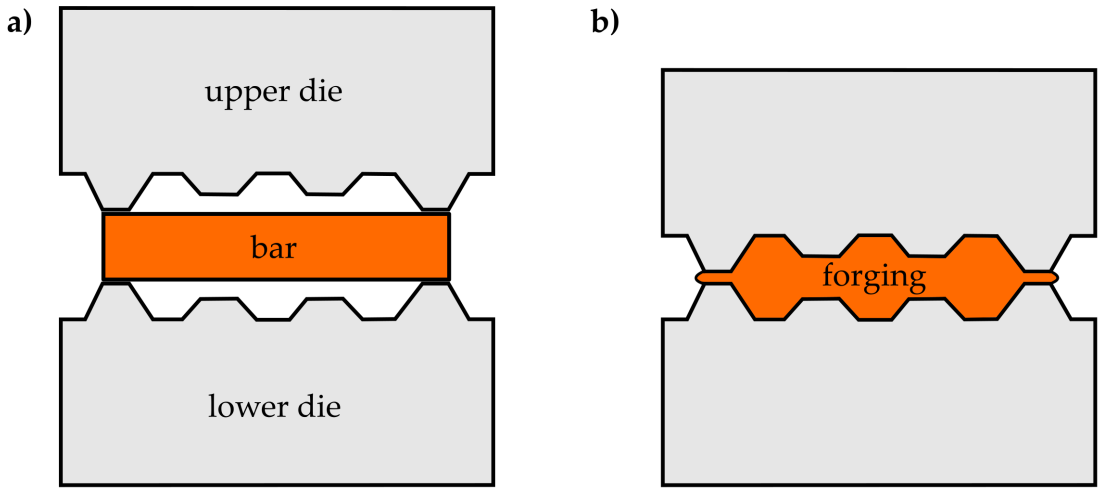

Figure 2.5: Schematic drawing of the closed-die forging process (modified after [9]). **a)** Bar between upper and lower die before the first forging step. **b)** After the first forging step a forging with flashes is obtained.

The forged and normalised rough crankshaft is finally shot blasted to clean the surface and inspected for cracks.

2.2.3.7 Machining

During machining, the rough crankshaft is machined at different parts. The ends are milled to the specified length and oil holes are drilled. The main journals are turned, turn-broached or rough ground while the pin journals are either milled or machined with the methods applied to the main journals. [7]

2.2.3.8 Induction Hardening

Induction hardening is only done on the crankshaft's pin and main journals surfaces which are the diameter, the radius and the sidewall. The two main objectives with this critical manufacturing step are i) increasing the wear resistance through hardening of the pin and main journals surfaces and ii) improving the fatigue strength through creation of desirable compressive stresses beneath the journals surfaces [7].

This is achieved by local induction heating of the defined surfaces. A coil is placed close to these surfaces and an alternating current is applied to the coil. The alternating current in the coil induces an alternating magnetic field in the workpiece. The alternating magnetic field in turn induces eddy currents of same frequency, but different direction as the current in the coil. The eddy currents produce heat in both coil and workpiece due to the Joule effect. Due to the skin effect, the density of eddy currents is higher just below the surface of the workpiece while it exponentially decreases in the direction away from the surface. [7]

Because of this, there is a temperature gradient in the workpiece: While the material just below the surface has high temperatures over autenitisation temperature Ac_3, the temperature further away from the surface is too low to affect the microstructure at all. Right after induction heating the material is quenched in oil which leads to high cooling rates. Under these conditions hard and brittle martensite is formed instead of the initial ferritic-pearlitic microstructure due to effects already mentioned in section 2.1.2.2 and 2.1.4. This transformation is also accompanied by a volume expansion which is responsible for the desired compressive stresses [7].

2.2.3.9 Tempering

After the oil quench, the material below the surface is hard and brittle and has high residual compressive stresses. These are desired, but can cause distortions in the finalising grinding process. On the other hand, the brittleness is undesired. To increase the toughness and to slightly reduce the residual stresses in the material close to the surfaces, the crankshaft is tempered at temperatures between 180-300 °C, i.e. far below Ac_1 (see Figure 2.4). This reduces the hardness to a certain extent as well. [7]

2.2.3.10 Grinding

Grinding is done on the main and pin journals surfaces in order to meet the requirements set on aspects like roundness, size and width and to create a smoother surface [7]. In this process, an abrasive wheel with hard material grits as geometrically undefined cutting edges, fixed by a bond, rotates at high speed. As soon as the hard material grits get in contact with the surface, they cut away chips from the surface and introduce heat by rubbing [4]. The grinding wheel quality, defined by e.g. the sharpness of the grits, and process parameters such as grinding wheel speed influence the respective shares of cutting and rubbing.

If the grinding process induces too much heat into the ground surface and the material beneath it, unfavourable consequences might occur: Grinding burns, caused by local thermal overload, change the microstructure in the affected area. This can result in either a local hardening that leads to cracks or to local tempering that makes the material even softer than after the intentional tempering process. This is not desired since the surface properties of the crankshafts bearing surfaces like hardness and residual compressive stresses are significantly decreased. [20]

To check the crankshaft for these undesired defects, several inspections and tests are performed. One of these is described in section 2.3.1. Grinding is the last manufacturing step performed on the investigated crankshafts. However, there is done superfinishing as a very last step to achieve very smooth surfaces [7].

When considering the grinding process the term *grindability* has to be mentioned. According to KALPAKJIAN and SCHMID [9], grindability can be defined as the ease of grinding a material taking into account considerations like quality of the produced surface, surface integrity, wheel wear, cycle time and also economic

aspects in general. This means that the cheaper the process and the better the output quality, the better the grindability of the material at a given set of grinding parameters.

2.3 Non-destructive Testing Methods

This section explains briefly the principles behind the two NDT methods that are relevant for the work described in this thesis. For further information and details professional literature is suggested.

2.3.1 Barkhausen Noise Analysis

The Barkhausen noise analysis (BNA) is a NDT method that is used for heat treatment verification and surface integrity since it correlated with hardness and residual stresses. BNA makes use of the Barkhausen noise, which is a electromagnetic phenomenon that is only found in ferromagnetic materials such as iron and steel [21].

Ferromagnetic materials consist of so called magnetic domains. Each domain has a magnetic orientation and is separated from differently oriented domains by domain or Bloch walls. If no magnetic field H is applied, these magnetic domains are randomly oriented and cancel each other out, the material is demagnetised. If a external magnetic field H is applied, the domains with preferred orientation grow while the other domains shrink. Therefore the domain walls move. However, this movement can be hindered by various obstacles which pin the domain walls until their energy is high enough to overcome the obstacle. Because of this, the movement of the domain walls always happens in discrete disruptive steps and not continuously. In a material with few obstacles, the domain walls are less hindered and thus the domain wall motion occurs in big steps. Thus, the magnetisation of the material increases/decreases in large steps as well. Such materials are referred to as magnetically soft and are magnetised and demagnetised with ease. In a material with many obstacles, the domain walls are hindered a lot and thus the domain wall motion occurs in small steps. Such materials are referred to as magnetically hard and are hard to magnetise and demagnetise. [22]

The disruptive steps of the domain wall motion and their magnitude can be recorded and are referred to as the Barkhausen noise (BN). Hardened steel e.g.

is a magnetically hard material that allows only slow movement of the domain walls and thus have a low BN while unhardened steel would have a high BN (see Figure 2.6 b)). Due to magnetostriction, the BN signal is influenced by residual stresses in the tested material. This effect can be used for indirect residual stress determination. Generally, compressive stresses lead to a low BN signal while tensile stresses lead to a high BN signal [21].

To perform a BNA on a material an alternating current is applied on a magnetisation yoke that generates an alternating magnetic field in the material. As a result of this, the domain walls are always moving. This will cause a BN signal. The BN signal from a certain position is detected by a BN detector and sent to the central unit that processes and saves the BN signal data. Figure 2.6 a) shows this process schematically. The analysing depth for the standard testing frequency and hardened and tempered steel as material is about 100 µm [23]. A deeper insight especially on BNA applied on crankshafts is given by TOMKOWSKI [22].

2.3.2 XRD Residual Stress Measurement

X-ray diffraction (XRD) can be used to measure residual stresses by using the interplanar spacing d_{hkl} of a crystal's hkl plane in the material as a measure of elastic strain. The background to this is *Bragg's law* which states that beams are in constructive interference if the path length $2d_{\mathrm{hkl}} \sin\theta$ is a whole number n of the beams wavelength λ. This is expressed by the formula [25]:

$$n\lambda = 2d_{\mathrm{hkl}} \sin\theta \tag{2.1}$$

Figure 2.7 a) shows Bragg's law of X-ray diffraction at crystal planes. The path length is dependent on the diffraction angle θ and the interplanar spacing d_{hkl} and is thus expressed with these terms in the formula. This means that, with a given wavelength λ, a change in interplanar spacing d_{hkl} has to result in a change of the diffraction angle θ. In the case of compressive residual stresses in a surface, the diffraction angle would increase compared to the unstrained state. The reduced interplanar spacing has its roots in elastic compressive strains which are caused by compressive stresses. [25]

The XRD residual stress measurement uses this relations to calculate residual stresses in the surface of work pieces. Figure 2.7 b) shows schematically the

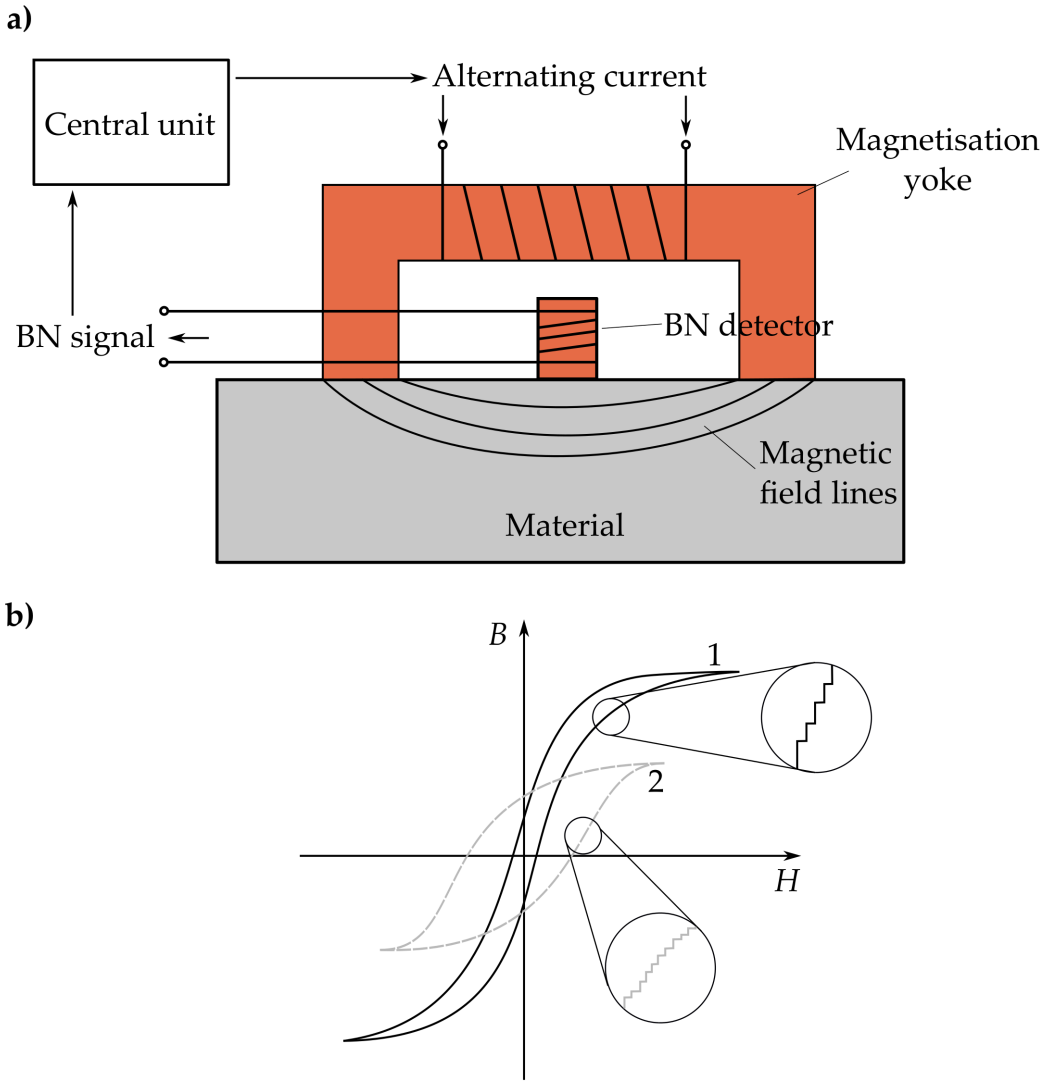

Figure 2.6: Schematic drawings of the BNA measurement set-up and BN in magnetically soft and hard materials. **a)** General schema of BNA measuring set-up (modified after [22]). **b)** Hysteresis loop and BN for a magnetically soft (1) and hard (2) material (modified after [23], [24]).

principle of the residual stress measurement. It is assumed that close to the surface only plane stresses and strains are present. So, the first interplanar spacing that is measured perpendicular to the workpiece surface can be assumed to be the interplanar distance for the unstrained condition. To spot the interplanar spacing in the direction of the residual stresses, either the sample or the X-ray source with the measuring head is tilted away from the normal position in the direction of the stresses that are to be analysed. At several tilting angles (at least 5 according to [25]) the interplanar spacing is measured as shown in Figure 2.7 b). In a compressive planar stress condition, the interplanar distance d_{hkl} will decrease with increasing tilting angles χ. When the interplanar spacing d_{hkl} is plotted against $\sin^2\chi$, a linearly decreasing line is obtained. Its slope and the materials linear elastic parameters like Young's modulus and Poisson's ratio allow the calculation of the residual stresses in the plane of tilting [26]. Further and more detailed information on residual stress measurement using XRD and in general are given by WITHERS and BHADESHIA [13] and FITZPATRICK et al. [25].

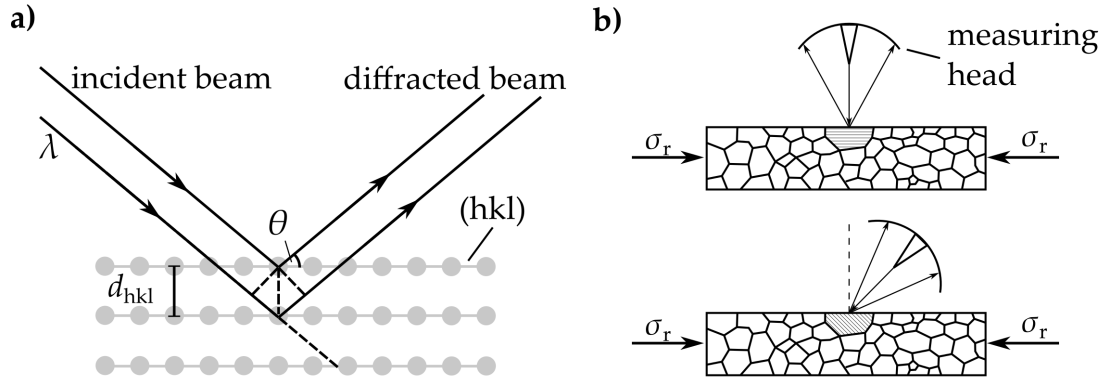

Figure 2.7: Schematic qualitative drawing of the XRD residual stress measurement. The stresses σ_{r} indicate the compressive stresses that are measured. **a)** Visualised Bragg's law (modified from [25]). **b)** Schematic drawings of an XRD measurement. Measuring head untilted (upper) and tilted (lower). The beam from the tilted head hits a differently oriented grain with lower interplanar spacing than in the image above due to the compressive stresses acting on it.

3 Methodology and Experimental Methods

3.1 Methodology

For the investigations the following items were available at the thesis project's start:

- two steel bars (one from a recycled batch and one from an ore-based batch, each from a different supplier)
- two crankshafts (recycled and ore-based, same batch as corresponding bar)
- Barkhausen Noise Analysis (BNA) data measured at the sidewalls of the crankshafts pin journals

The methodology that was followed during the master thesis project is illustrated in the floating diagram in Figure 3.1. The investigations were divided in two parts: One part was dealing with the initial bars made from ore-based and recycled steel, the other with the forged and ground crankshafts made from ore-based and recycled steel. Both crankshafts were the first crankshaft ground after dressing of the grinding wheel and were ground using the same parameters.

The investigation on the steel bars was focused on their microstructure. The differences between the ore-based and recycled steel bars in characteristics such as present phases, grain size and banding were of interest. Knowing the characteristics of the starting materials for crankshaft manufacturing was considered crucial, since it provides information on the input material treated throughout the whole crankshaft manufacturing.

The investigations on the crankshafts were limited to the crankshafts sidewall surfaces, since they are reported to be most prone to thermal damage caused by grinding. The decision on where investigations should be performed was based on

the examination of the BNA data that were available for the pin journals sidewalls. Since a higher BN should correlate with lower hardness and lower compressive residual stresses, BN serves as a measure to assess surface integrity and thus grindability as well. By comparing the BNA data trend of ore-based and recycled steel crankshafts from their pin sidewalls, specific areas of interest at the sidewalls were chosen for further investigation and treatment. Interesting areas were the ones with either larger difference in BN or similar BN. As a result of this, one side of both ore-based and recycled crankshaft pin V6 where chosen for investigations at the positions α_{BN} of 45°, 135° and 180°. The location of these positions on pin V6 F-side is shown in Figure 3.2.

These positions where investigated with following methods and under following objectives:

- Residual stress measurement using XRD to check the residual stresses just below the sidewall surface
- Sample preparation for optical microscopy and scanning electron microscopy
- Nital etch of prepared samples to make present phases visible, optical microscopy
- Picric acid etch of prepared samples to make prior austenite grains visible, optical microscopy, prior austenite grain size estimation conforming the ASTM standard E112 - 13
- Scanning electron microscopy for observation of hardened areas with higher magnification
- Vickers hardness testing conforming ASTM standard E92 - 17 to examine the hardness close to the sidewall surface and in the depth profile

The results of these methods are discussed and a conclusion is drawn finally.

3.2 Experimental Methods

3.2.1 Optical Microscopy on Steel Bars

To perform optical microscopy on samples from the steel bars a slice from every steel bar was cut. The bars slices were cut with the *Struers* cut-off machine *Discotom-*

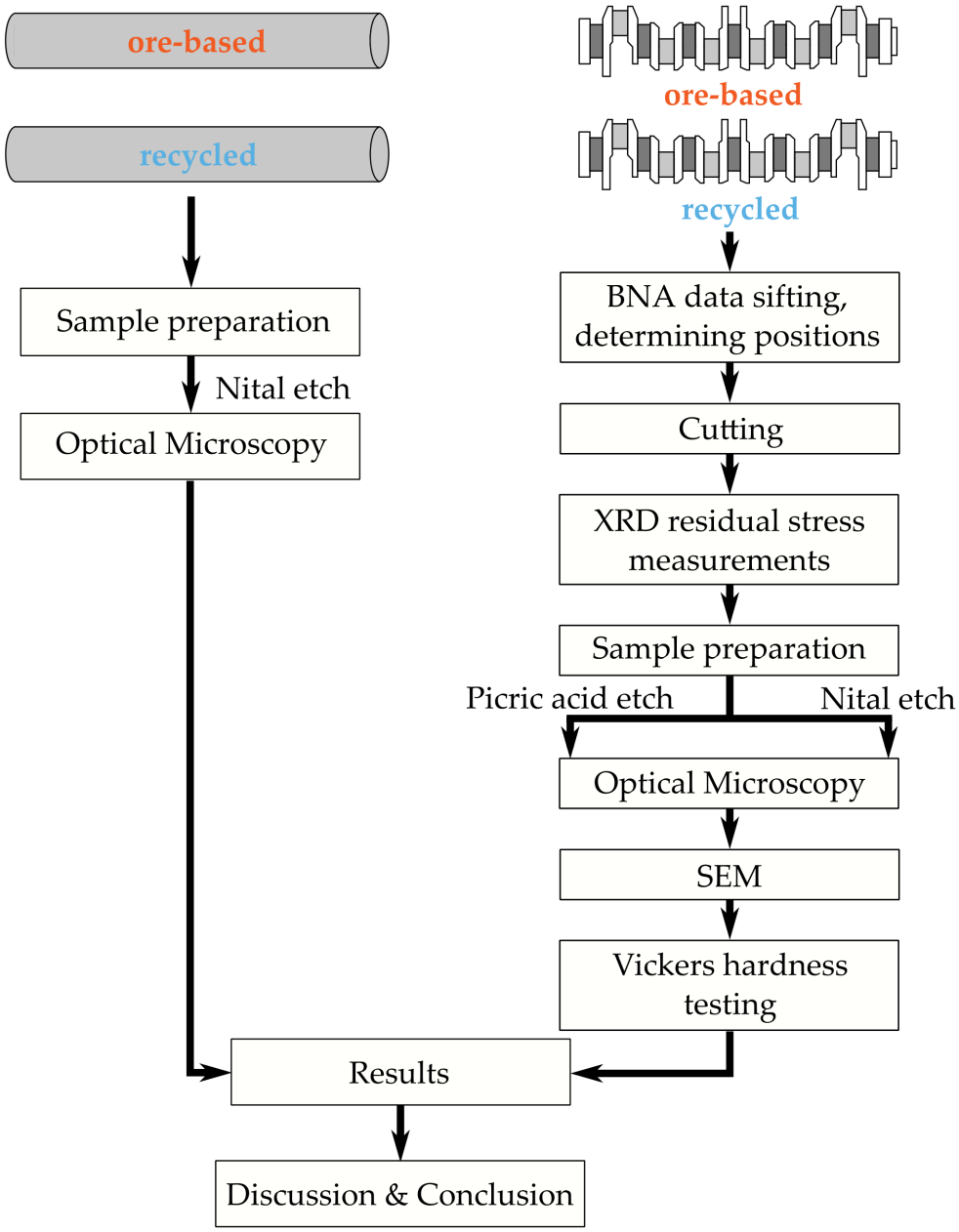

Figure 3.1: Floating diagram on the methodology followed during the master thesis project.

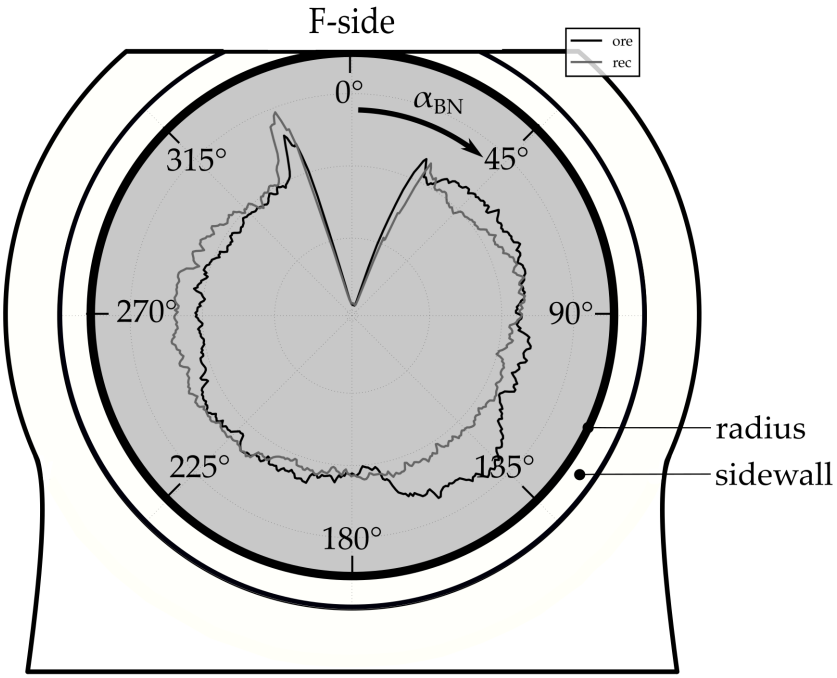

Figure 3.2: Pin V6 F-side. BNA data obtained from measurements along the sidewall of pin V6 F-side are projected in the part with the corresponding BN measurement angle α_{BN}. Figure 3.4 shows how this part is obtained from the sectioning procedure.

2 using the cut-off wheel *40A25* for soft steel. Figure 3.3 shows schematically how samples are obtained from the steel bars. First, a horizontal cut was made resulting in a disk section, followed by two vertical cuts resulting in a rod. A final horizontal cut at the bottom of the rod led to the steel bar samples. To ensure that the rolling direction is visible in the microstructure, the surface marked in Figure 3.3 has to face towards the cylinders lateral surface. The samples were mounted in conductive mounting resin *Polyfast* from *Struers*, using *Struers* mounting press *CitoPress-20* small sample slot with a diameter of 30 mm. Grinding and polishing was performed on *Struers* grinding/polishing machine *TegraPol-31* in single sample mode. The grinding and polishing parameters are given in table A.1 in Appendix 1. The samples were etched with *Nital* etchant containing 3 % nitric acid until surface etching was apparent.

3.2.2 XRD Residual Stress Measurement on Pin Journal Sidewalls

The large cuts through the pin journals' diameters, indicated with dashed lines in Figure 3.4 a) and b), were done at the automotive company. To protect the

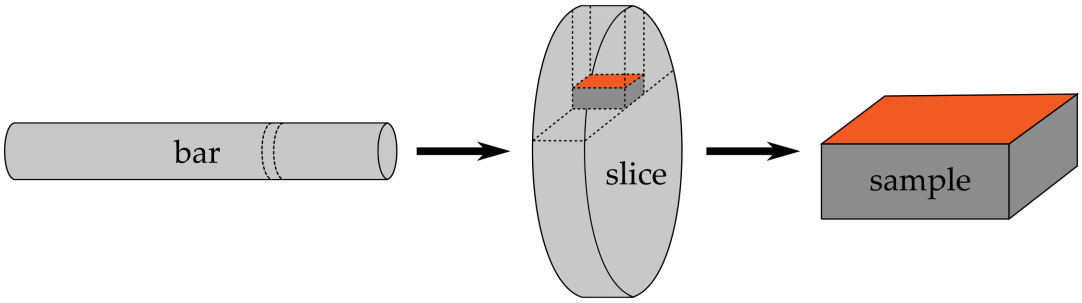

Figure 3.3: Schematic drawing of the sample sectioning procedure performed on the steel bars. A slice is cut out from the steel bar. From this slice the final sample is obtained.

sidewall surface from damage such as corrosion it was coated with a sprayed varnish before cutting. The cutting resulted in two parts containing a sidewall. One closer to the F-end, thus called F-side and another one closer to the T-end called T-side.

The varnish was removed after the cutting. Little position markers ($d_\mathrm{p} = 3\,\mathrm{mm}$ were stuck on the positions where residual stress should be measured (see Figure 3.5). This was supposed to ensure that the right positions are measured with a minimal deviation from the positions that were analysed by BNA and all the methods used during the project. The such prepared F-side of the pin journal V6 was then transferred to the residual stress measuring device *X-ray Stress Analyser 3000 G2R* by *Stresstech*.

The F-side part was placed in a way that the sidewall surface of the to be analysed position was perpendicular to the incident X-ray beam hitting the position in the center of the position marker. Figure 3.6 shows schematically the set-up of the residual stress measurement. In a) the top view is sketched. Three rotation angles ϕ have been used. The residual stresses measured at rotation angle $\phi = 0°$ are the residual stresses in grinding direction. For each position 8 tiltings in both + and -χ angle were done.

Before measuring the residual stresses of the samples a calibration was performed using a ferrite calibration sample and calibrating for the $(2\,1\,1)$ crystal plane. As a X-ray source a chromium source was used. The position of the short detectors was placed in a way that the beam diffracted by $2\theta = 156.1°$ could be fully detected. The incident beam passed a collimator with a 1.5 mm orifice.

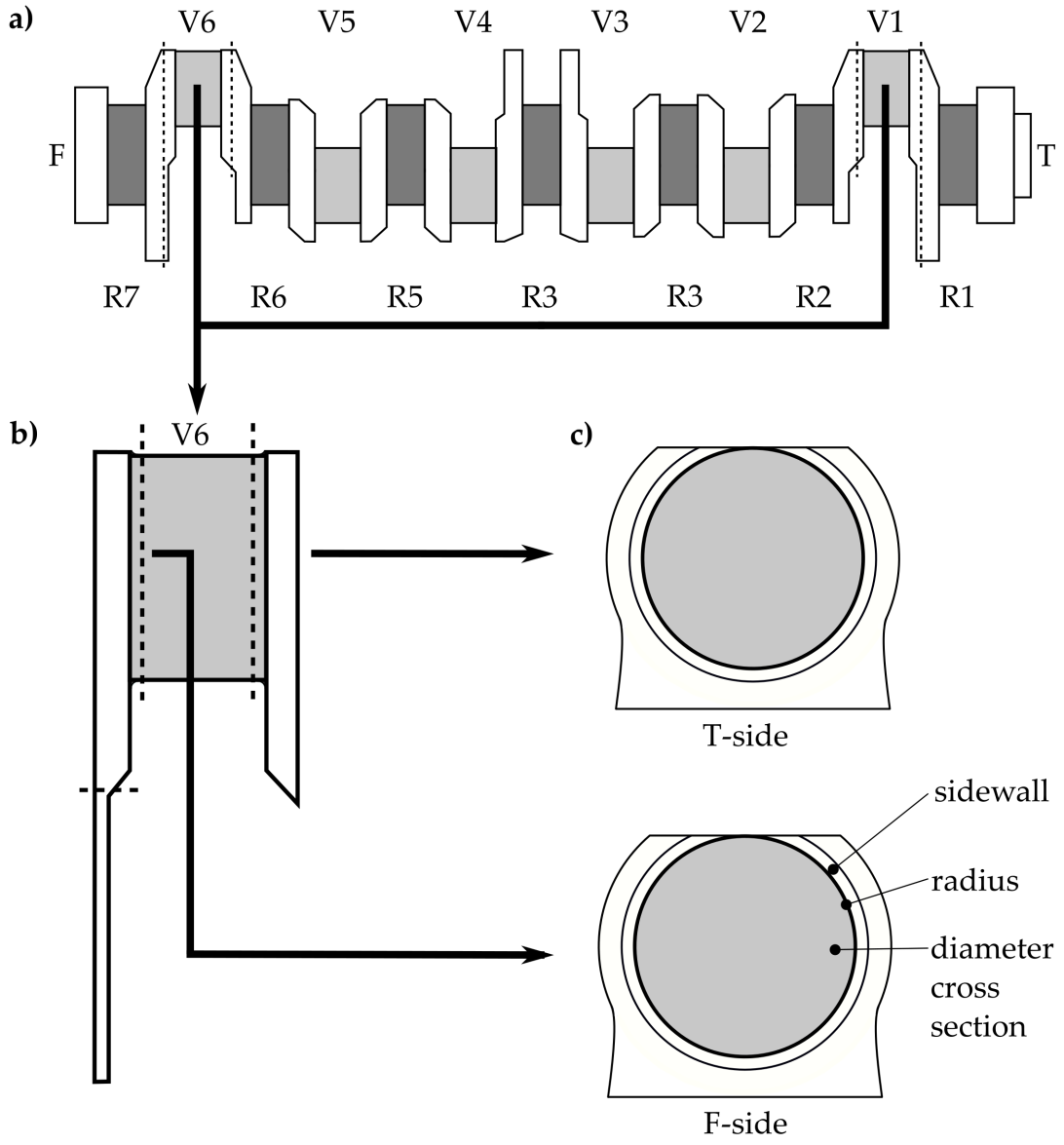

Figure 3.4: Schematic drawing of the sample sectioning procedure performed on the crankshafts and pin journals. **a)** Crankshaft with an F-end and a T-end, main journals (R1...R7) and pin journals (V1...V6): Cutting out pin journals V1 and V6. **b)** Cut out pin journal: Cutting away obstructive web parts. Cuts as close as possible to both sidewalls. **c)** Pin journal T- and F-sides with accessible sidewall and radius.

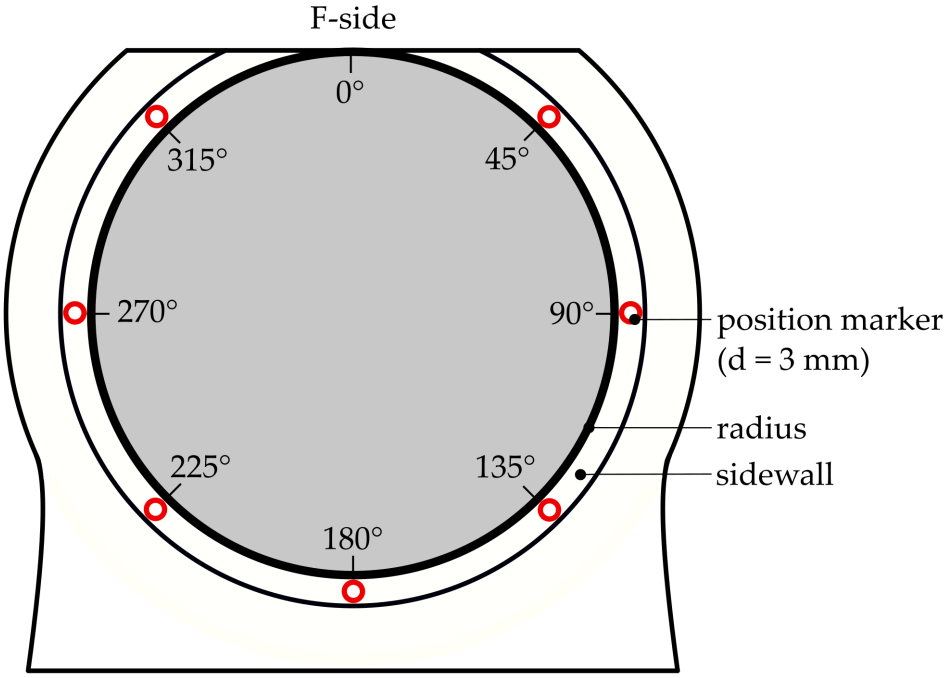

Figure 3.5: Schematic drawing of a F-side sample prepared for residual stress measurement using XRD. Every spot to be analysed is marked with a position marker. This enables a higher precision of hitting the same spots that were analysed by BNA. The corresponding angle value is added to every marker. For a T-side, the angle values increase anti-clockwise.

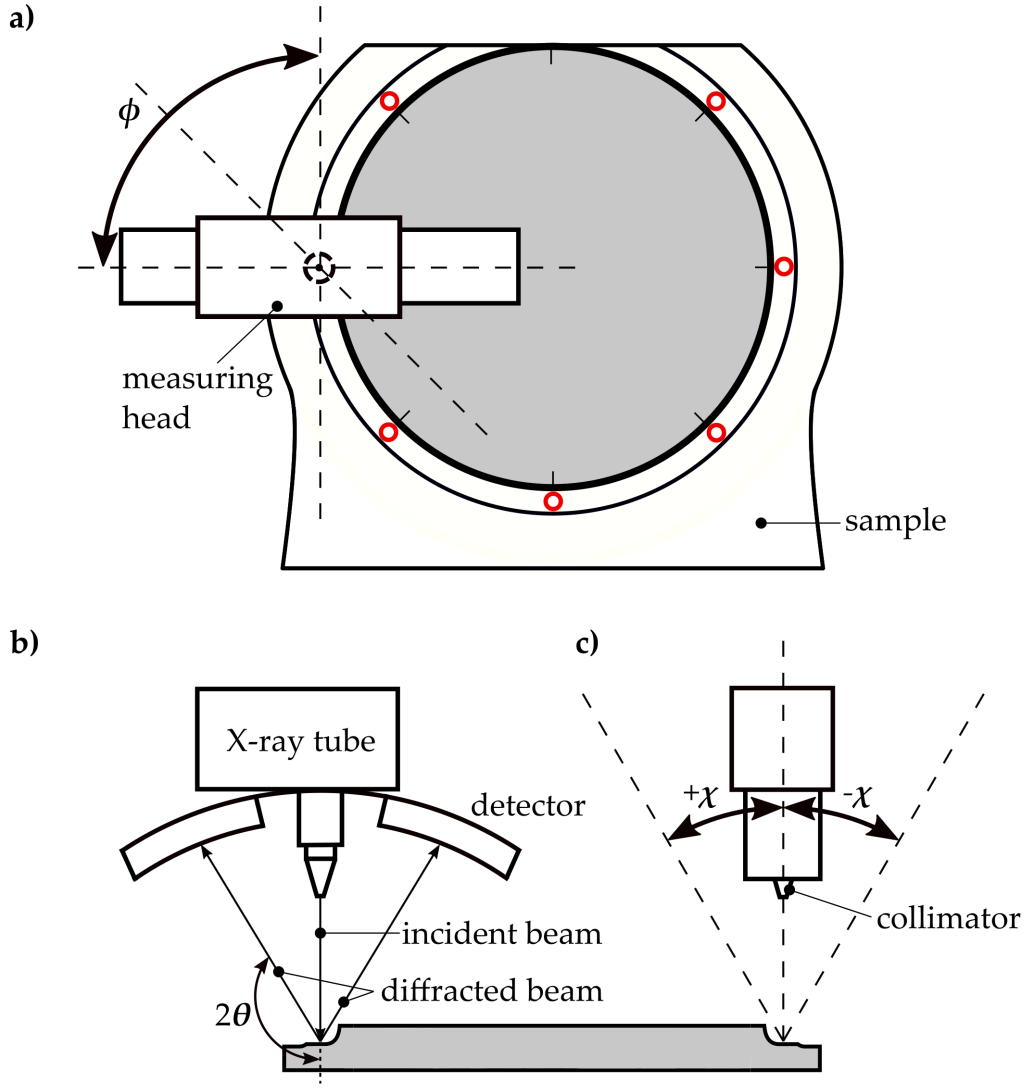

Figure 3.6: Schematic drawing of the set-up and parameters of residual stress measurement using XRD. **a)** Top view: Sample with measuring head containing X-ray tube, collimator and detectors above it. The rotation angle ϕ is indicated. In the image the rotation angle $\phi = 0°$. **b)** Side view: Sample lying flat and measuring head in $\phi = 0°$ position above it. The Bragg or diffraction angle 2θ is indicated. **c)** Side view: Sample lying horizontally and measuring head in $\phi = 90°$ position above it. The tilting angle χ is indicated.

3.2.3 Microscopy on Sidewalls

As shown in Figure 3.7 a), the disk-shaped pin journal sample is cut through the pin journal diameter's center. By this a sector for each marked position is obtained (see Figure 3.7 b)). The sectors are cut with the *Struers* cut-off machine *Discotom-2* using the cut-off wheel *50A25* for hardened steel. The final cut that created the later to be analysed surface was made with the *Isomet 2000* precision saw by *Buehler* using the *50A13* cut-off wheel by *Struers*. Mounting, grinding and polishing follows the procedure already described in section 3.2.1.

Etching was performed in two different ways. Etching the samples surface with *Nital* etchant revealed the phases in the material. After this etching process, the samples were investigated through both optical and scanning electron microscopy. Following these investigations the last two steps of polishing shown in table A.1 in Appendix 1 were applied on the samples to prepare them for the next etching: Etching with a picric acid etchant revealed the prior austenite grains and their grain boundaries for the prior grain size estimation described in section 3.2.5. This picric acid etchant contained a saturated aqueous picric acid solution with added sodium dodecylbenzene-sulfonate as wetting agent and hydrogen chloride (1 mL per 500 mL of saturated aqueous picric acid solution). The samples were etched for 5 min at about 80 °C. Subsequent manual low-pressure polishing was done to reduce unessential etching details and to make the prior austenite grain boundaries more visible in contrast to the grains interiors.

3.2.4 Optical Microscopy on Pin Journal Bulk

To obtain samples of the pin journals bulk, further away from the hardened area, the section piece from the sectioning procedure described in section 3.2.3 and shown in Figure 3.7 were used. As shown in Figure 3.8 the lower, triangular piece was used for further sectioning. Two parallel vertical cuts, one precisely in the middle, the other slightly on the side, were performed to obtain the sample (Figure 3.8 b) and c)). Mounting was done as already described in section 3.2.1 but using the large sample slot with a diameter of 40 mm instead due to the large sample size. Grinding and polishing was performed according to the approach summarised in table A.1 in Appendix 1. After grinding and polishing the samples were etched with *Nital* etchant containing 3 % nitric acid until surface etching was apparent.

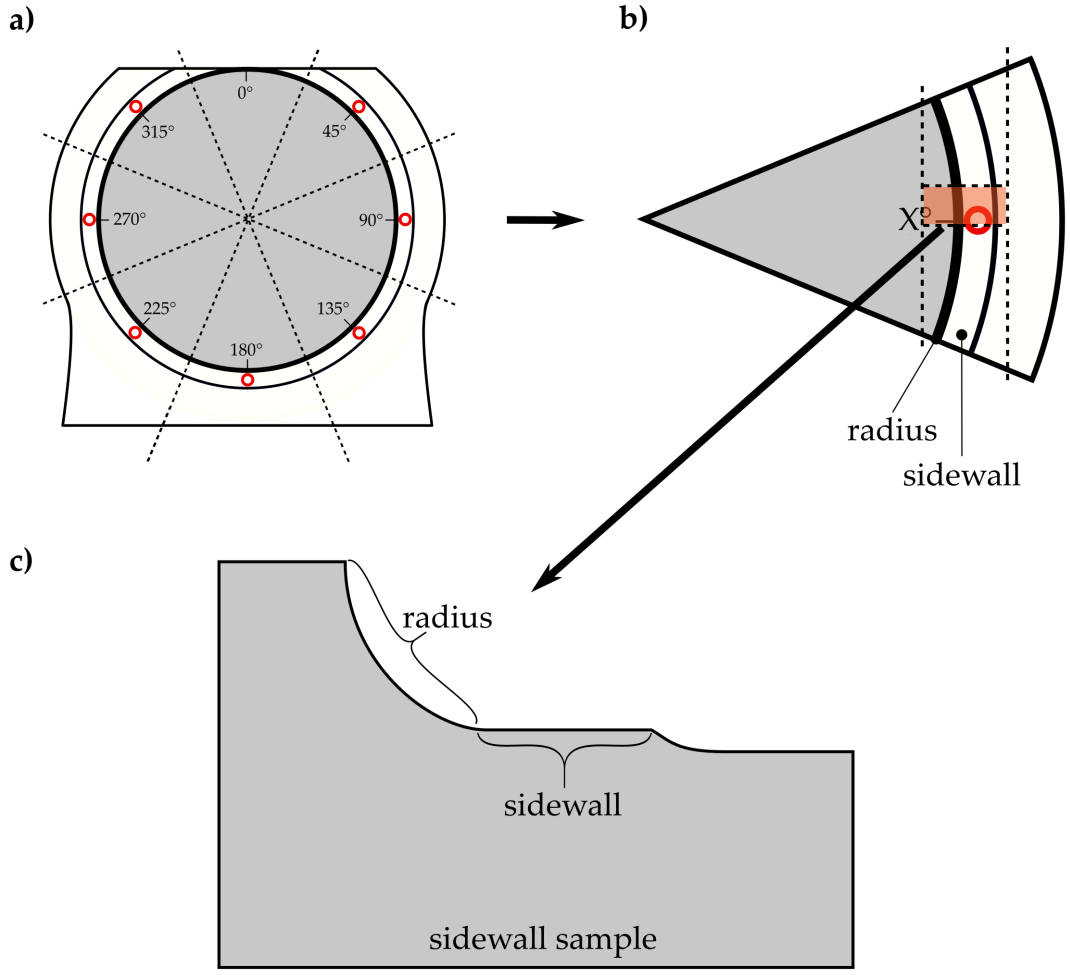

Figure 3.7: Schematic drawing of the sample sectioning procedure performed on an F-side of a pin journal. **a)** Cutting the pin journal F-side through the diameter center. **b)** Cutting part from X° position obtained from the cutting described in a). **c)** Side view on the part obtained from the cutting described in b).

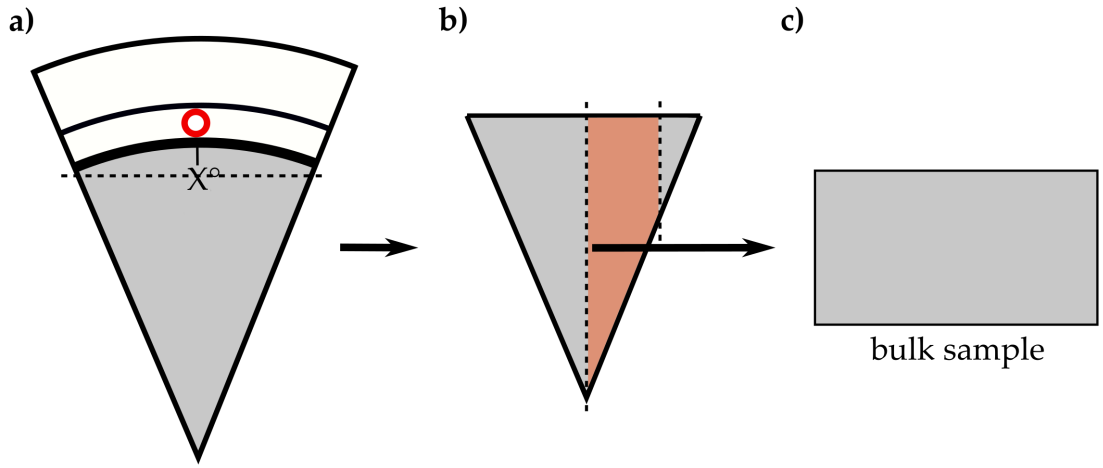

Figure 3.8: Schematic drawing of the sample sectioning procedure performed on F-side of pin journal part from X°. **a)** Using the triangluar part resulting from step b) in Figure 3.7. **b)** Cutting part. **c)** Side view on part obtained from step described in b).

3.2.5 Average Prior Austenite Grain Size Determination

The prior austenite grain size was estimated using the micrographs from the picric acid etched samples and applying the Heyn Lineal Intercept Procedure described in the standard *ASTM E112-13 Standard Test Methods for Determining Average Grain Size* [27]. The Heyn Lineal Intercept Procedure was applied on 4 images per sample with 5 lines of $l = 300\,\mu m$ length each. Like this the required minimum 50 interceptions N per image, i.e. at least 10 interceptions per line, were reached. Per line this means at least 10 interceptions N_l. The distance between the lines was chosen to be at least 20 µm. Per line, the average grain size was calculated as follows: $d_{\gamma,e} = \frac{l}{N_l}$. From all the 20 values of average grain size estimates $d_{\gamma,e}$ per sample an arithmetic average and standard deviation were calculated.

3.2.6 Vickers Hardness Testing on Sidewalls

Vickers hardness testing is performed using the *DuraScan 70G5* hardness testing machine by *emco-test*. The pyramid-shaped Vickers indent is pressed with a defined test-load F into the sample surface. The softer the material at the surface and the volume below, the larger is the indent impression and vice versa.

The hardness is calculated by the *ecos Workflow* software using the length of the two diagonals d_1 and d_2 in millimetres and the test load F in kilograms-force applied

on the surface. With the diagonals d_1 and d_2 the mean diagonal d is calculated, so that the hardness is obtained as follows:

$$\mathrm{HV} = 1.8544 \times \frac{F}{d^2} \tag{3.1}$$

For each sidewall sample two Vickers hardness methods were used. The first method used an applied force $F = 0.3$ kgf. This relatively low load enabled measuring the hardness of the material as close to the sidewall surface as possible while still testing in accordance with the standard. The indents were set in two parallel rows of 25 indents as close to each other and the surface as recommended, i.e. $2.5d$ for the distance between sidewall surface and $3d$ for the distance between the indents (see Figure 3.9). In this way, the hardness close-to-sidewall was determined.

The second method used an applied force $F = 5$ kgf. This required wider distanced indents. These indents were set in two parallel rows of 9 indents perpendicular to the sidewall surface. Their distance was $3d$ (see Figure 3.9). In this way, the hardness depth profile from the sidewall was measured.

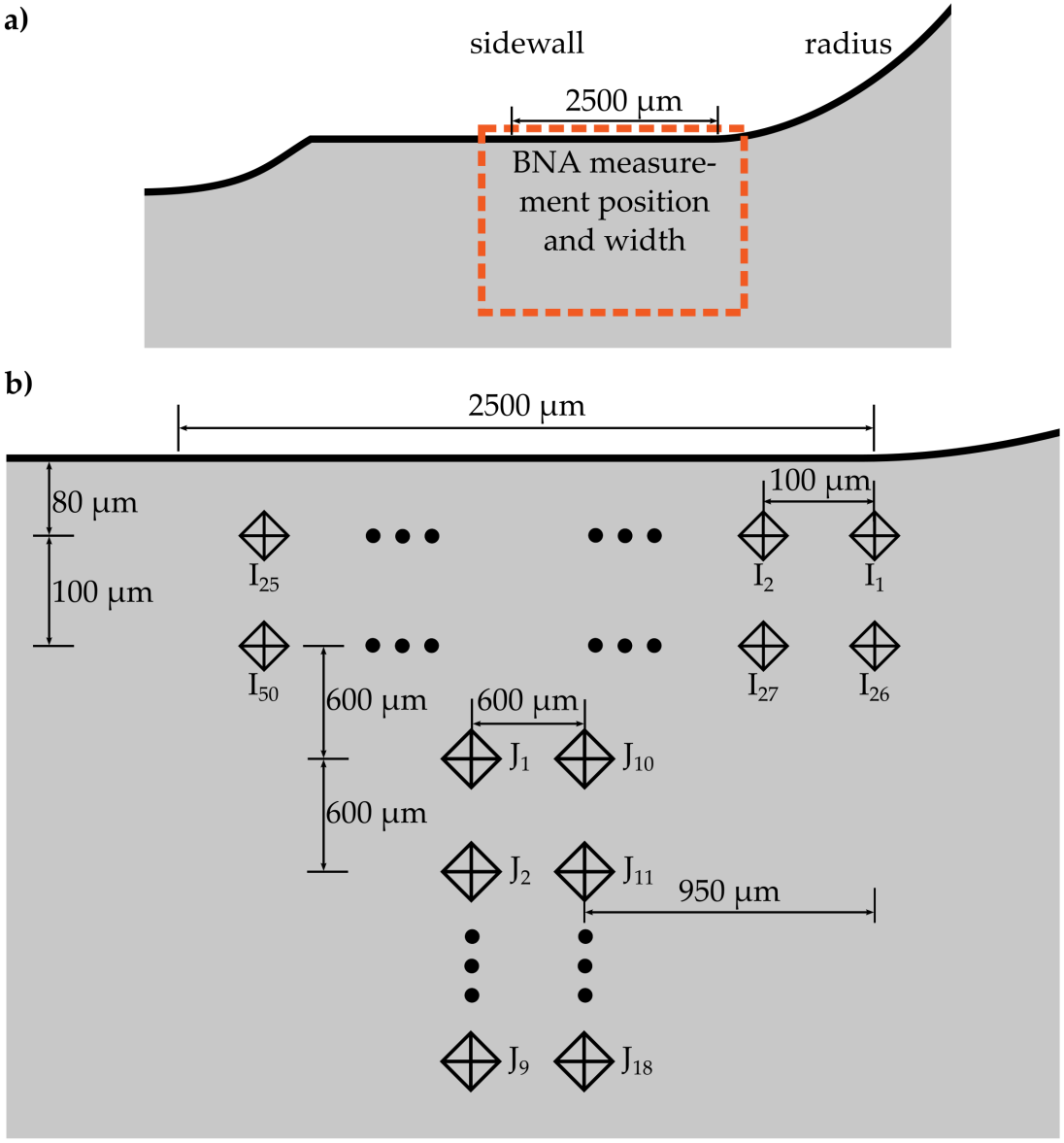

Figure 3.9: Schematic drawing of Vickers hardness testing design on sidewall samples (not to scale). **a)** Cutout from the schematic drawing of the sidewall sample (see Figure 3.7 c)). By measuring 2500 µm from the point were the radius ends and the sidewall begins the width and measuring position of the BNA sensor is determined. **b)** Coutout from a). All indents I have a centre-to-centre distance of 100 µm to each other and a distance of 80 µm from their centre to the sidewall surface. The indents J have a centre-to-centre distance of 600 µm to each other and to the indents I. The two rows of indents J are positioned with given distance to each other around the middle fo the BNA measuring width.

4 Results

4.1 Microstructure of Steel Bars

The light microscopy on the steel bars reveals their microstructural characteristics: Both steels share a ferritic-pearlitic microstructure where a network of ferrite grains binds pearlite grains as shown in Figure 4.1. However, the size of the pearlite grains differ significantly: When comparing the microstructure of the ore-based steel bar (Figure 4.1 a)) with the microstructure of the recycled steel bar (Figure 4.1 b)) it is evident that in the recycled steel much coarser pearlite grains and a much coarser ferrite network formed than in the ore-based steel. However, the ferrite grains and the pearlite colonies in the pearlite grains do not seem to be much different when comparing the ore-based and recycled steel.

This trend of larger pearlite grains is also revealed by the Figures 4.1 c) and d). While the ore-based steel shows very fine pearlite grains compared to the recycled steel where these grains appear very coarse. Another aspect revealed in that figure is the banding in the microstructure. There are horizontally oriented bands that are either richer in ferrite or pearlite. This anisotropy and inhomogeneity seems to be less visible in the recycled steels microstructure. Another indicator of the banded microstructure is the elongated inclusions that appear seldom, randomly in the microstructures of both steels. These also share the orientation in the same direction as the banding.

4.2 Microstructure of Crankshafts

4.2.1 Microstructure in Unhardened Areas

The light microscopy performed on the unhardened areas from the crankshaft bulk reveals further aspects. As in the bars, the microstructure in the bulk is ferritic-

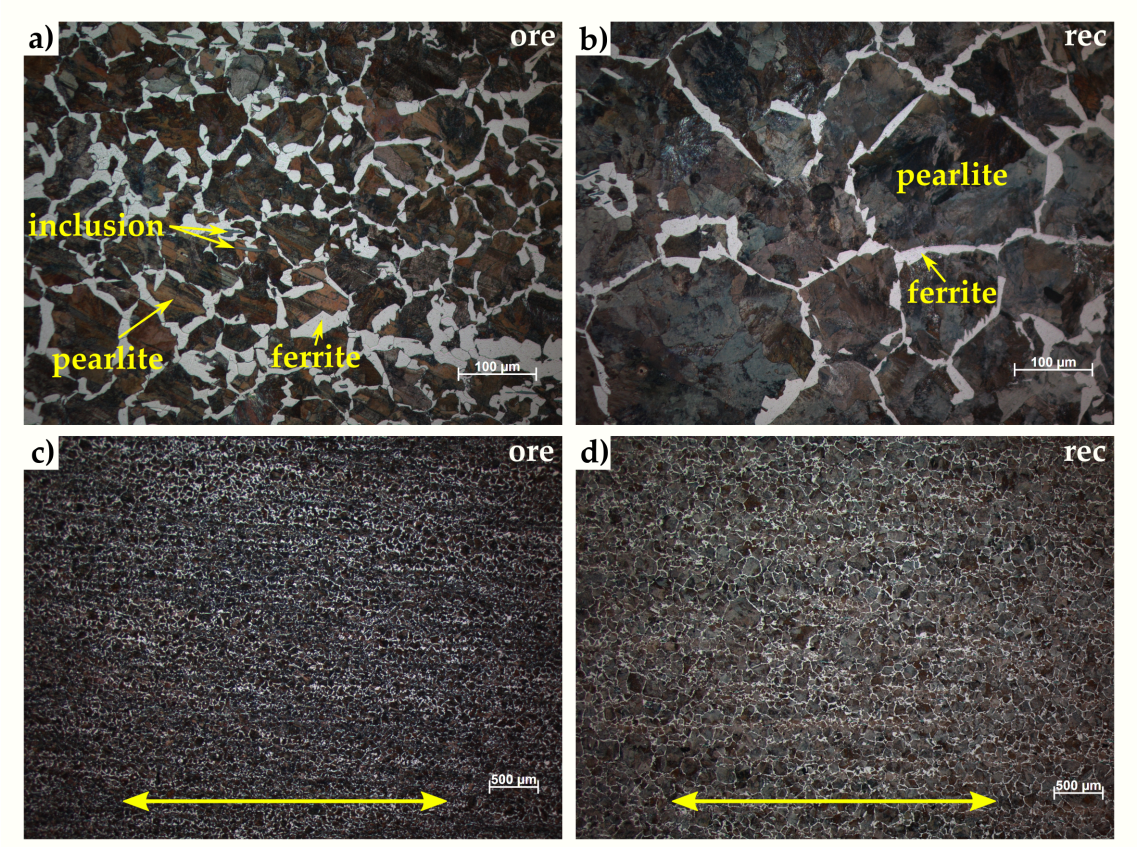

Figure 4.1: Light micrographs of the steel bars, nital etched. **a)** Ore-based steel, ferrite and pearlite indicated. **b)** Recycled steel, ferrite and pearlite indicated. **c)** Ore-based steel, rolling and banding direction indicated with arrow. **d)** Recycled steel, rolling and banding direction indicated with arrow.

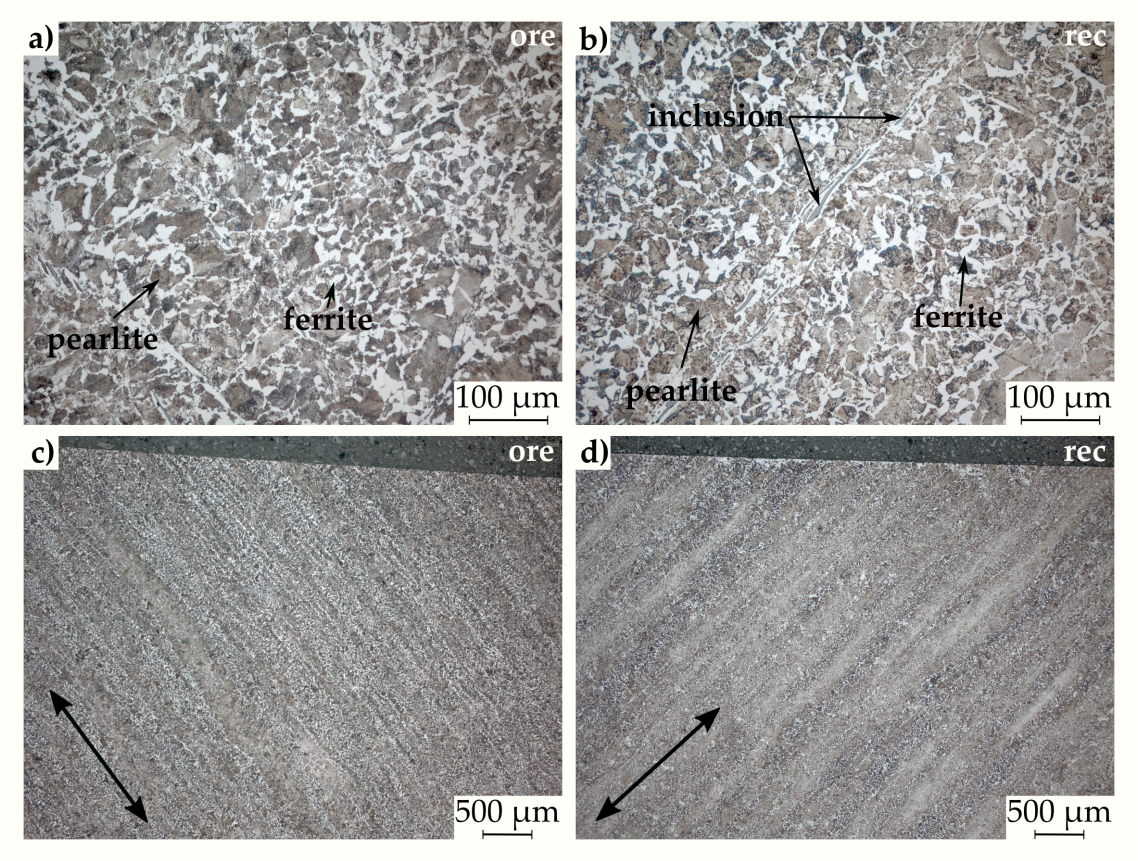

Figure 4.2: Light micrographs of crankshaft bulk, nital etched. **a)** Ore-based, ferrite and pearlite indicated. **b)** Recycled, ferrite and pearlite indicated. **c)** Ore-based, banding direction indicated with arrow. **d)** Recycled, banding direction indicated with arrow.

pearlitic as shown in Figures 4.2 a) and b). The banding in the microstructure is still present which is clearly visible in Figures 4.2 c) and d). However, the microstructure in the micrograph in Figure 4.2 d) for the recycled steel appears much more inhomogeneous than the microstructure in the micrograph in Figure 4.2 c) for the ore-based steel. In the first, broader and brighter bands aligned in banding direction are in apparent contrast to the surrounding microstructure, while in the latter, bands are visible but they are not standing out due to low contrast or size. In Figure 4.2 b) strongly elongated inclusions are visible.

Another aspect is the grain size, especially the pearlite grain size: While there is an obvious and large difference in pearlite grain size in the steel bars, the difference is not existing in the crankshafts bulk microstructure. A comparison of the micrographs a) and b) in both Figures 4.1 and 4.2 shows that clearly. Moreover, the grain sizes are not only more similar, but also generally reduced when compared with the grain sizes in the bars.

4.2.2 Microstructure in Hardened Areas

Figure 4.3 shows micrographs recorded from the crankshafts sidewall at the position $\alpha_{BN} = 45°$ in different magnifications. Images a) and b), which represent the lowest magnification, show an overview over the whole sample surface. The hardened and unhardened area can be clearly distinguished. It seems, that the hardened area in the recycled steel sample reaches deeper from the surface into the material than in the ore-based sample. More details can be found in section 4.4.

There is no distinct banding in both ore-based and recycled steel sample. However, the recycled steel sample appears more inhomogeneous than the ore-based steel sample: There is a higher contrast in the brownish colors in the hardened area. Darker dots and brighter areas are quite notably zoned from the surrounding area. This can be observed even in the images c) and d) of higher magnification.

The images e) and f) show the martensitic structure of both ore-based and recycled sample just below the sidewall surface. In contrast to the images above, differences are hardly found in the martensitic microstructure. There are no indications of different sizes of the martensitic structures or a kind of inhomogeneity. The martensite structures that formed inside the prior austenite grains are randomly oriented. The size of the prior austenite grains where the martensitic structures form plays a role for the resulting martensite structure sizes, as already stated in section 2.1.2.2 in the Background chapter. Therefore the prior austenite grain size was investigated (see section 4.3).

Figure 4.4 shows micrographs recorded from the crankshafts sidewall at the position $\alpha_{BN} = 135°$ in different magnifications. The overview over the whole sample surface of both ore-based and recycled is shown in the images a) and b). There is a clear contrast between the hardened martensitic area and the unhardened ferritic-pearlitic area. As discussed about the previous sample, the hardened area in the recycled steel sample seems to reach deeper from the surface into the material than in the ore-based sample. In contrast to the findings based on Figure 4.3, there is a clear banding in both ore-based and recycled steel sample. The recycled steel sample appears again more inhomogeneous than the ore-based steel sample: While the ore-based sample has few narrow and brighter bands and few broad and darker bands drawing through the hardened area, the recycled sample appears to consist of many bright and dark bands aligned next to each other as also shown in the images c) and d) of higher magnification. The difference in homogeneity and banding is also visible in the unhardened area.

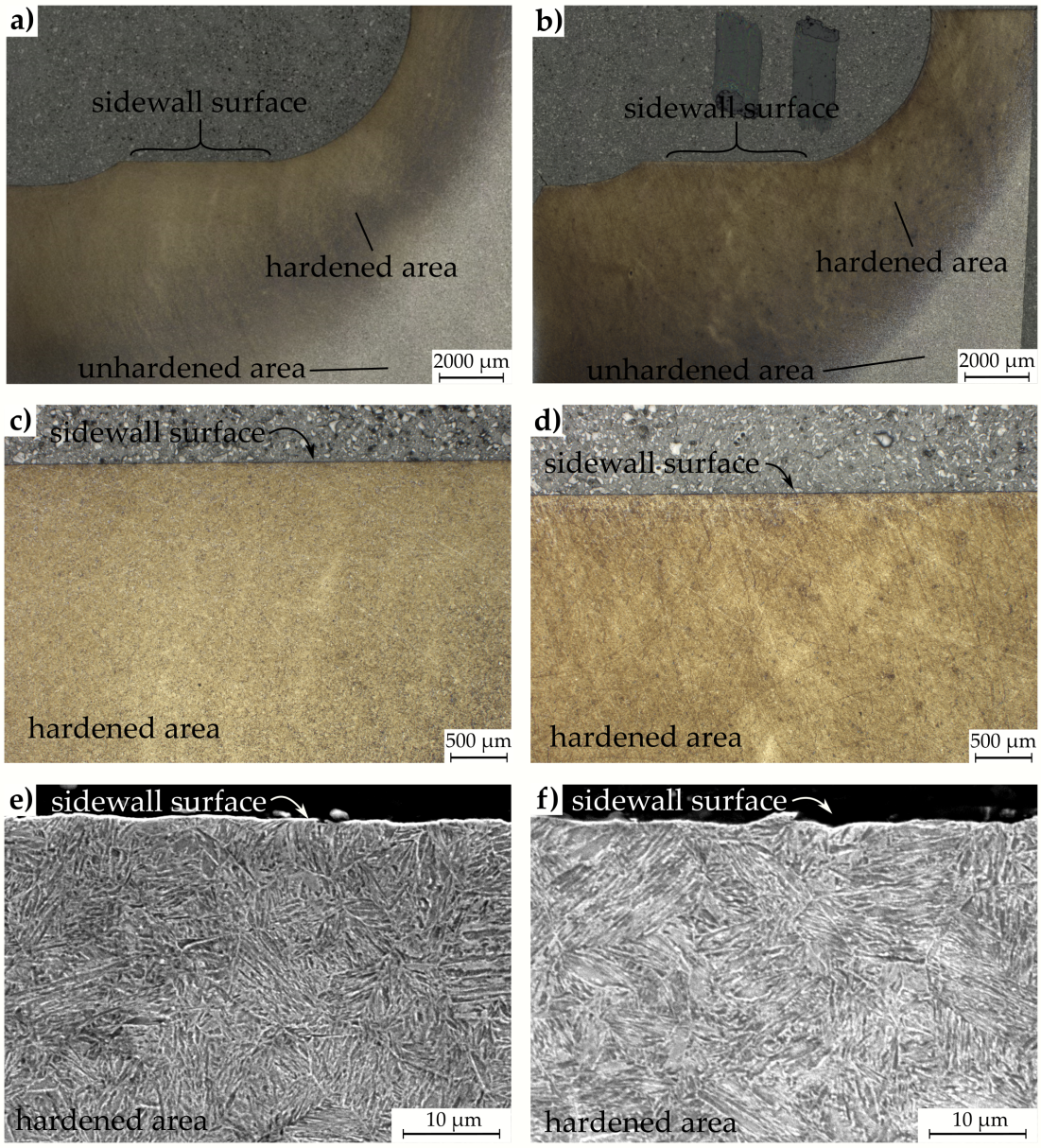

Figure 4.3: Micrographs of ore-based and recycled steel crankshafts sidewall cross section of pin no. 6 F-side at $\alpha_{BN} = 45°$. All micrographs were obtained on Nital etched samples. **a)** Ore-based, light micrograph. **b)** Recycled, light micrograph. **c)** Ore-based, light micrograph. **d)** Recycled, light micrograph. **e)** Ore-based, SEM micrograph. **f)** Recycled, SEM micrograph.

The images e) and f) show the martensitic structure of both ore-based and recycled sample just below the sidewall surface. As in the discussion on the previous sample, it is not possible to detect major differences in the martensitic structure. Hence, it should be referred to section 4.3 that deals with the prior austenite grain size estimations.

The micrographs taken from the crankshafts sidewall at the position $\alpha_{BN} = 180°$ in different magnifications are shown in Figure 4.5. The overview over the whole sample surface of both ore-based and recycled is shown in the images a) and b). As discussed about the previous two samples, the hardened area in the recycled steel sample seems to reach deeper from the surface into the material than in the ore-based sample. In contrast to the findings based on Figure 4.3, there is a clear banding in both ore-based and recycled steel sample as already observed in Figure 4.4. The recycled steel sample appears again more inhomogeneous than the ore-based steel sample. However, the contrast difference between the ore-based and recycled steel sample is not as pronounced here as in the samples from position $\alpha_{BN} = 135°$, but it is still visible. While only few brighter bands draw through the hardened area the ore-based sample, in the recycled sample there are many clearly zoned bands being in a stronger contrast to the surrounding. The images c) and d) show this plainly. The difference in homogeneity and banding is also visible in the unhardened area (see Figure 4.5 a) and b)).

The images e) and f) show the martensitic structure of both ore-based and recycled sample just below the sidewall surface. As in the discussion on the previous samples, it is not possible to detect significant differences in the martensitic structure. Hence, it should be referred to section 4.3 that deals with the prior austenite grain size estimations.

4.3 Prior Austenite Grain Size Estimation

The results of the grain size estimation are shown in Figure 4.6, in which for every position α_{BN} the prior austenite grain size estimate from the ore-based and the recycled sample is plotted as bars. At first glance it is obvious that the estimated prior austenite grain size is clearly increasing with increasing position angle α_{BN}. The estimated prior austenite grain size for a certain position however is not varying much between ore-based and recycled steel: The mean values for the estimated prior austenite grain size of the one steel are always within the narrow

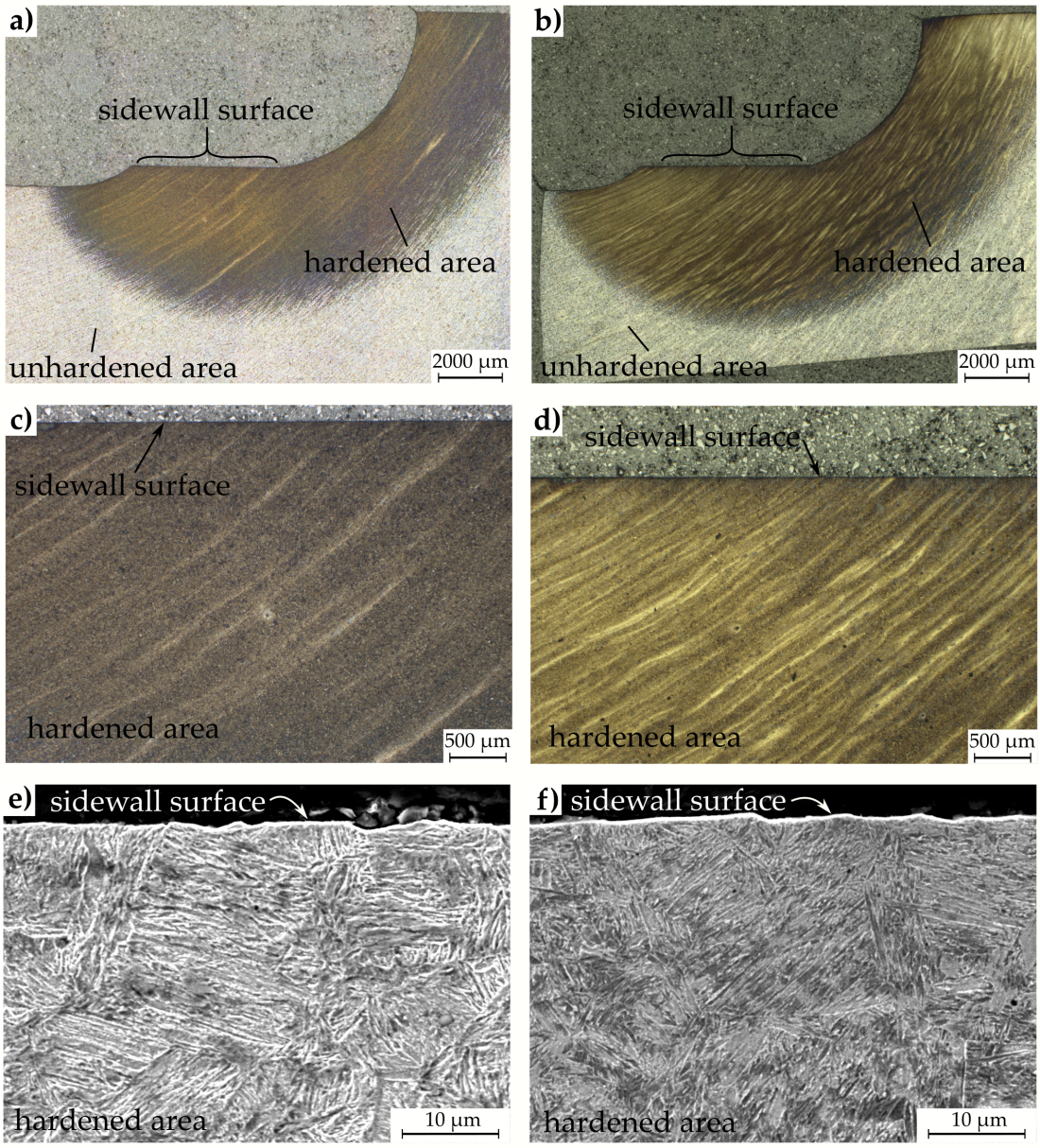

Figure 4.4: Micrographs of ore-based and recycled steel crankshafts sidewall cross section of pin no. 6 F-side at $\alpha_{BN} = 135°$. All micrographs were obtained on Nital etched samples. **a)** Ore-based, light micrograph. **b)** Recycled, light micrograph. **c)** Ore-based, light micrograph. **d)** Recycled, light micrograph. **e)** Ore-based, SEM micrograph. **f)** Recycled, SEM micrograph.

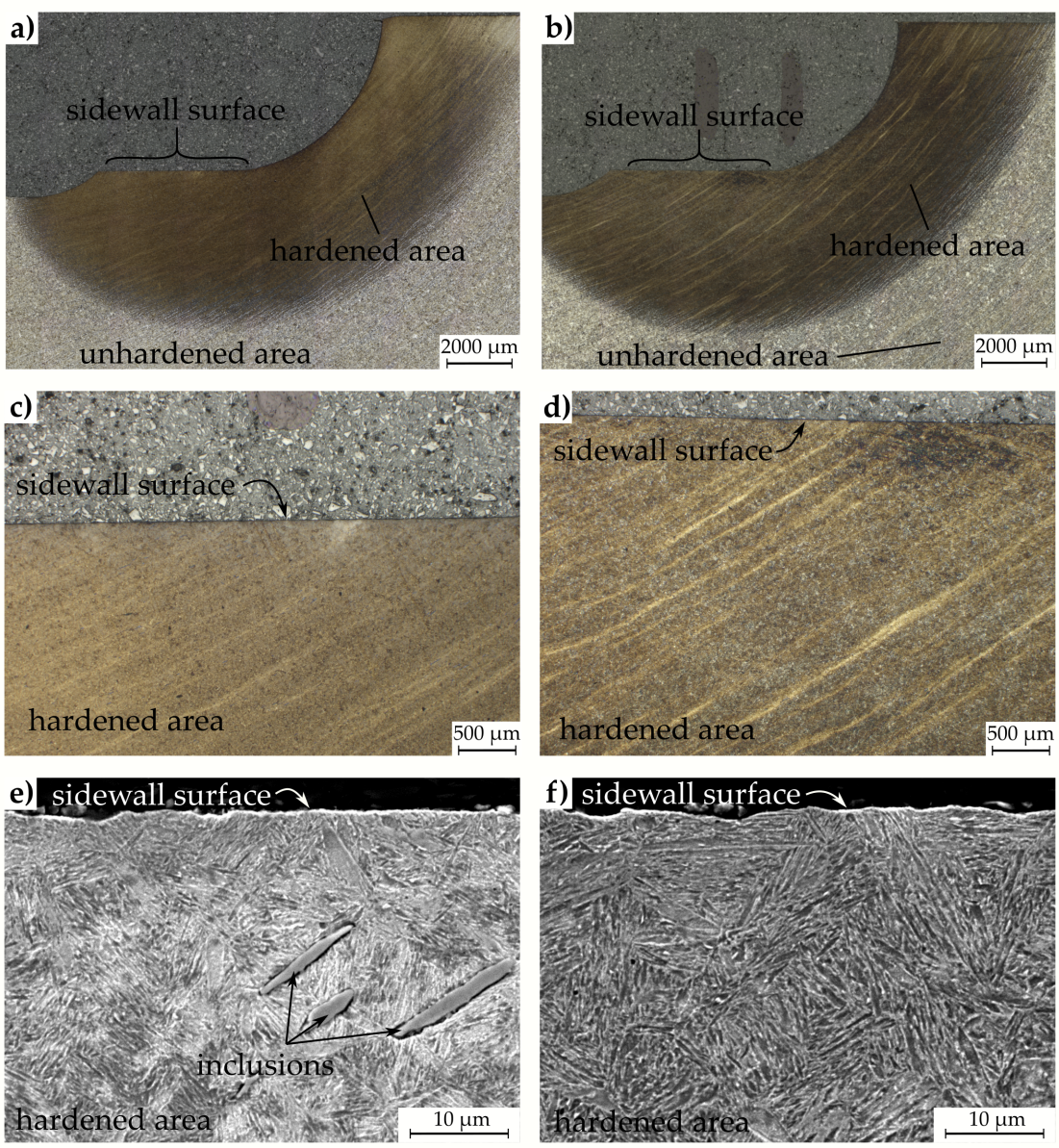

Figure 4.5: Micrographs of ore-based and recycled steel crankshafts sidewall cross section of pin no. 6 F-side at $\alpha_{BN} = 180°$. All micrographs were obtained on Nital etched samples. **a)** Ore-based, light micrograph. **b)** Recycled, light micrograph. **c)** Ore-based, light micrograph. **d)** Recycled, light micrograph. **e)** Ore-based, SEM micrograph. **f)** Recycled, SEM micrograph.

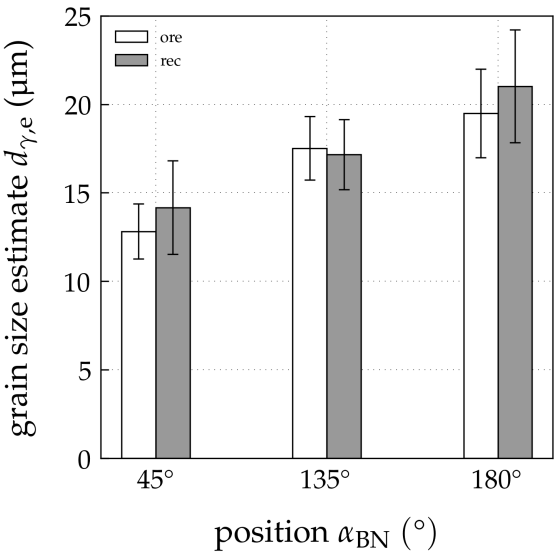

Figure 4.6: Prior austenite grain size estimate $d_{\gamma,e}$ in ore-based and recycled steel crankshaft pin sidewall, plotted against the position α_{BN}.

standard deviation of the other. So it can be said that the investigated samples suggest that there is no significant variation of prior austenite grain size when comparing the two steels, but instead when comparing the positions where the samples were taken from the crankshaft.

Figure 4.7 shows examples of some micrographs that served as the base for the prior austenite grain size estimation. The images a) to d) show that there are larger prior austenite grains in the samples taken at the $\alpha_{BN} = 180°$ position than at the $\alpha_{BN} = 45°$ position.

4.4 Hardness and Hardenability at the Sidewall

The hardness close to the sidewall surface does not show distinct differences neither between the two steel batches nor the different positions. The hardness of both steels at all positions is about 550 HV 0.3. While the recycled steel seems to be slightly harder at the positions $\alpha_{BN} = 45°$ and $\alpha_{BN} = 135°$, the ore-based steel is somewhat harder at position $\alpha_{BN} = 180°$ (see Figure 4.8). All in all, the hardness close to the sidewall has to be considered as similar.

In contrast to the hardness close to the sidewall, the results from the hardness depth profile show a clear difference: First, the hardness curves of both steels

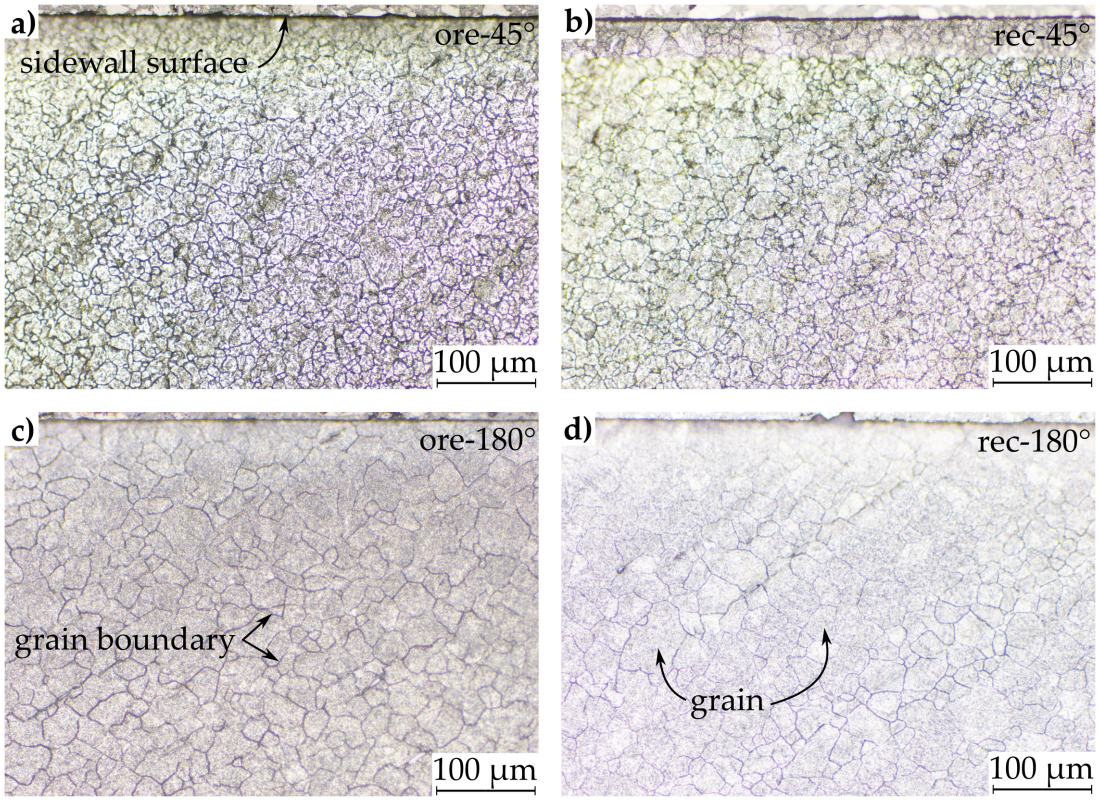

Figure 4.7: Examples of micrographs, picric acid etched, used for prior austenite grain size estimation via Heyn Lineal Intercept Procedure. **a)** Ore-based, position $\alpha_{BN} = 45°$. **b)** Recycled, position $\alpha_{BN} = 45°$. **c)** Ore-based, position $\alpha_{BN} = 180°$. **d)** Recycled, position $\alpha_{BN} = 180°$.

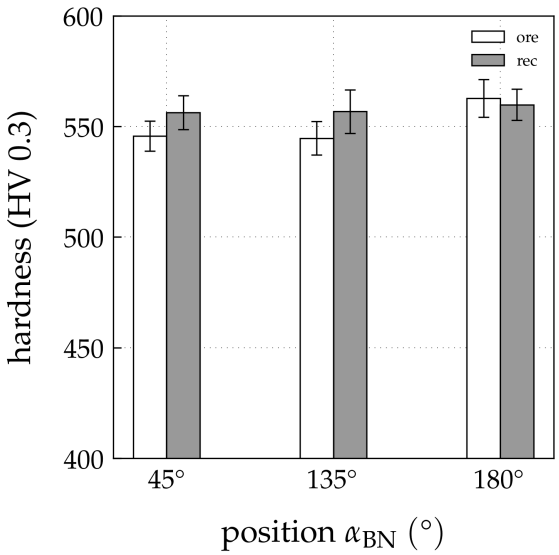

Figure 4.8: Hardness HV 0.3 close-to-sidewall in ore-based and recycled steel crankshaft pin sidewall, plotted against the position α_{BN}.

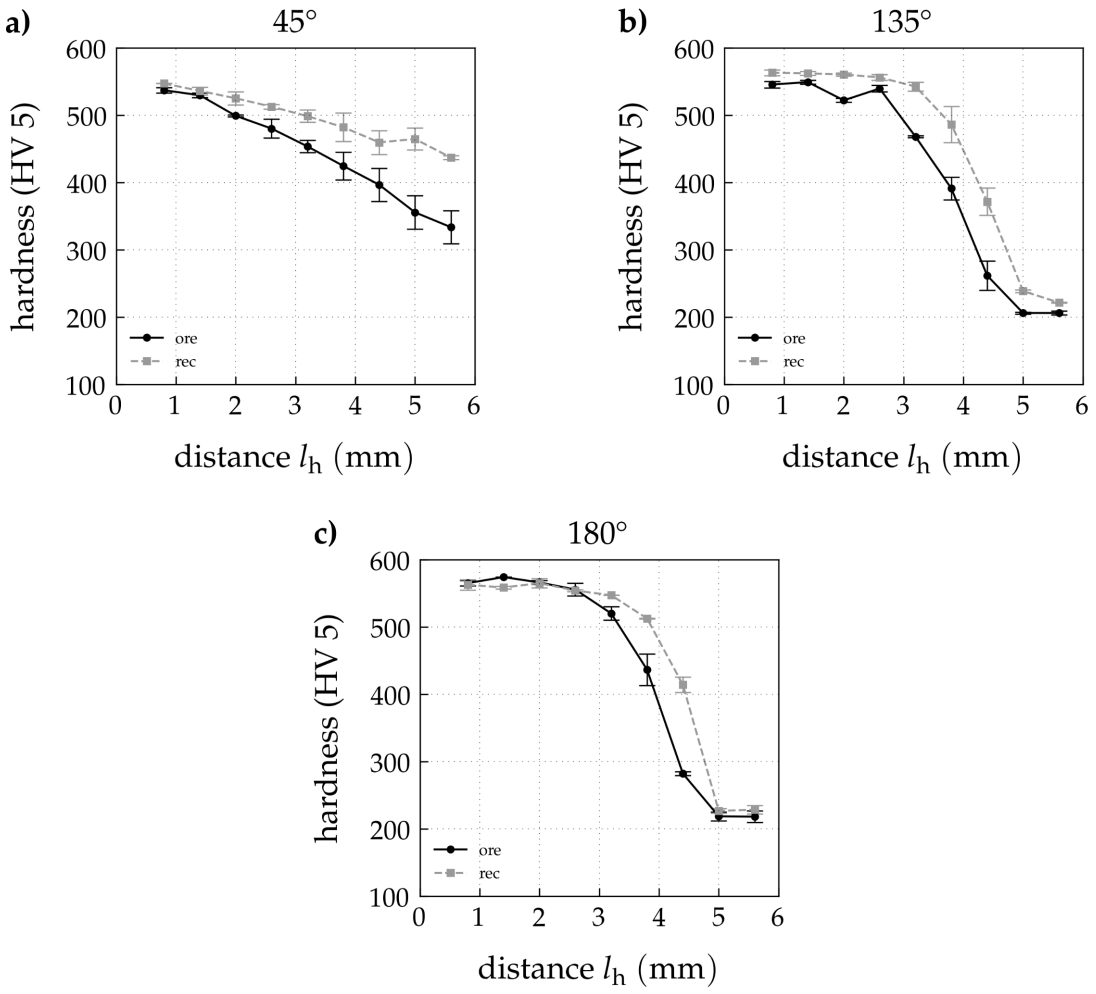

Figure 4.9: Hardness HV 5 plotted against the distance from the hardened sidewall surface l_h of ore-based and recycled steel crankshaft pins. **a)** Position $\alpha_{BN} = 45°$. **b)** Position $\alpha_{BN} = 135°$. **c)** Position $\alpha_{BN} = 180°$.

in the images in Figure 4.9 start a similar hardness of about 550 HV. However, with increasing distance l_h from the sidewall surface the hardness decreases for both steels, but the recycled steel has a higher hardness at distances further away from the sidewall. In images b) and c) it is obvious that the hardness gradient is relatively strong and that at distances higher than 5 mm the curves for both steels again reach the same hardness level slightly above 200 HV. The curves in image a) however show a different shape. They indicate an almost linear decrease of the hardness. At the distance of 5 mm the hardness for the ore-based steel is below 350 HV and for the recycled steel below 450 HV.

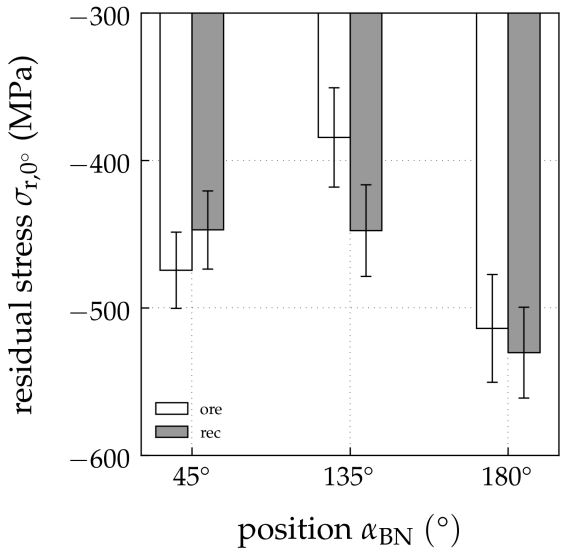

Figure 4.10: Residual stress $\sigma_{r,0°}$ in grinding direction in ore-based and recycled steel crankshaft pin V6 sidewall, plotted against the position α_{BN}.

4.5 Residual Stresses in the Sidewall Surface

The results from the residual stress measurements using XRD are shown in Figure 4.10. All the residual stresses in the grinding direction are compressive. However, their magnitude differs significantly between the different positions and even between the ore-based and the recycled steel. At the position $\alpha_{BN} = 180°$ the residual stresses do not differ much with values of about $-510\,\text{MPa}$ for the ore-based steel and $-530\,\text{MPa}$ for the recycled steel. On the other hand, at the position $\alpha_{BN} = 135°$ the residual stresses are generally lower when compared with the ones at position $\alpha_{BN} = 180°$, but with residual stresses of about $-380\,\text{MPa}$ for the ore-based steel and $-450\,\text{MPa}$ for recycled steel, the difference between the two steels at the same position is very significant. The residual stresses at the position $\alpha_{BN} = 45°$ are located between the ones of the other positions. The difference between the ore-based and recycled steel is very low and only at this position the ore-based steel shows higher compressive residual stresses than the recycled steel.

5 Discussion

A very significant difference between the ore-based and the recycled steel is found in the initial steel bars microstructure. The reason for these differences have to have their origin in the steel bars production. As KRAUSS states in [6], the austenitic microstructures response to hot-working processes like hot-rolling comprises various mechanisms of deformation, recovery, recrystallisation and grain growth. For high hot-working temperatures for example, the austenite grain size increases due to grain growth. Certainly, the hot-rolling temperature, cooling profile and the degree of deformation play a role for the final microstructure. These factors should be considered as the main reasons for the different pearlite grain sizes and the overall appearance of the microstructure. However, the most likely assumption is that the recycled steel bars were hot-rolled at higher temperatures than the ore-based steel bars which led to larger austenite grains that during cooling transformed to pearlite grains after ferrite precipitated at the austenite grain boundaries. The banding in the microstructure is very likely to arise from the hot-rolling process.

Despite the differences being very apparent in the bars, the forged and unhardened microstructure in the crankshafts does not show these differences. The grains size in both ore-based and recycled steel is reduced and similar. The reason for this is to be found in the forging process itself as well as in the normalising process that is undertaken to refine the microstructure after forging. In that sense it can be said that the normalising process made the microstructure of both steels more similar in the crankshafts and that the initial differences were reduced, assuming that the observations made in the bars apply for the bars the crankshafts were made of. However, the inhomogeneous appearance of the recycled steel microstructure remains as a distinct difference between it and the ore-based steel.

While no differences can be found in the microstructure of ore-based and recycled steel in the bulk of the crankshafts by visual inspection of the corresponding micrographs, quite distinct microstructural differences can be observed between ore-based and recycled steel when visually inspecting the hardened area at the

sidewall and the unhardened area close to it. The martensitic and ferritic-pearlitic microstructure of the ore-based steel appears more homogeneous than in the recycled steel. The microstructures were visualised by etching resulting in revealing of the phases which have different colors visible under the optical microscope. The different colors of particular bands in the hardened area indicate a different etching effect at different sites of the samples due to gradients in chemical composition. According to KRAUSS [6] this is related to the sluggish diffusivity of the substitutional alloying elements in the steel. Complete homogenisation to eliminate these chemical composition gradients takes long time and high temperatures and is therefore generally not undertaken in commercial steel processing.

Another aspect that should be mentioned is described by BERNS [3]: He refers to banding as a microstructural anisotropy that can result in direction-dependent properties that affect metal-working. When considering the sidewall micrographs it is clearly visible that the bands are oriented at an angle of about 45° towards the sidewall surface. Now when taking into account that the recycled material is less homogeneous and thus has a more distinct banding, this would mean a higher anisotropy that affects metal working operations like grinding. The aspects discussed in the following however do not support the concept that the recycled steel is less grindable than the ore-based steel.

No differences were found in the martensitic structures in the hardened areas of the sidewall. To get better information on the martensite structures the prior austenite grain size was estimated applying the Heyn Lineal Intercept Procedure on picric acid etched samples taken from the sidewall. According to KITAHARA et al. [8] the prior austenite grain size affects the packet size, i.e. the size of the martensitic structures. Small grain sizes again are generally related to higher strength and hardness as described by the Hall-Patch relation. The results from the prior austenite grian size estimation show that they are similar at a fixed position for both ore-based and recycled steel. A bigger variation however is to be found between the different positions: While at the position $\alpha_{BN} = 45°$ the mean prior austenite grain size estimation is around 13 µm, for position $\alpha_{BN} = 135°$ the mean prior austenite grain size estimation is around 17 µm and for position $\alpha_{BN} = 180°$ even around 19 µm. This slight increase of the austenite grain size with increasing position angle α_{BN} can be related to the forging and normalising process. As KRAUSS [6] states, due to high forging temperatures the austenite grains grow to coarse grains, but due to the complex forging shape (as it is the case in crankshaft forging) the degree of deformation varies within the forged part. As a result,

grains in some areas experience more deformation leading to a higher dislocation density. In the normalising process this could favour the nucleation of more and thus smaller new austenite grains than in less deformed areas. It is very likely a process-induced difference that is not related to the steel batch. In the end, the variation is also not very distinct and does not seem to affect the hardness either.

As already mentioned, both steels show a comparable hardness at small distances from the sidewall surface and also very close to the sidewall surface. However, the hardness profiles differ clearly. The recycled steel has a better hardenability when the depth of the hardening is considered as a measure. This can be a clear indicator for not only local compositional differences in every crankshaft (banding), but also for a compositional difference between the ore-based and recycled steel. If assumed that the process parameters of the performed induction hardening (austenitising temperature, austenitising time and cooling) are the same for both steels, a composition difference is the most likely reason for different hardenability.

The residual stresses at the different positions show a quite broad variation. The ore-based steel has lower compressive stresses at two positions and higher compressive stress at one position. There is a tendency that the magnitude of compressive residual stresses is more dependent on the position they were measured than on the material. This could have its roots in the grinding process. Inhomogeneous mechanical plastic deformation is induced by many randomly oriented and sized abrasive grains bond together to a grinding wheel and cutting off chips from the surface by fast rotation of the grinding wheel touching the work piece. This inhomogeneous mechanical plastic deformation is the major factor in the formation of residual stresses in ground components [12]. Grinding is usually accompanied by heat generation. It is imaginable that there are spots that are more affected by heat than others due to the grinding wheel character, geometrical inequalities at the sidewall surface and different approachability of several positions for the processing coolant etc. Thus resulting in different residual stresses in the ground sidewall surface. If the coolant is not able to cool the ground work piece properly, residual stresses can change and turn from compressive to tensile due to phase transformation, as already described in the case of hardened steel in section 2.1.4. It does not seem that this happened to any of the investigated positions since all samples show a martensitic microstructure below the sidewall surface. But a slight tempering might have taken place especially in the ore-based steel at position $\alpha_{BN} = 135°$.

A limitation of measuring residual stresses with XRD in the used setup is definitely the low analysing depth. Only stresses in the first micrometres beneath the surface are analysed while the stresses at deeper sights below the sidewall surface remain unrevealed. Thus, it is not reasonable to discuss the correlation of the residual stresses with the measured hardness, since the information on it was obtained from the material further below the sidewall. To correlate the residual stresses and the hardness either the residual stress measurement has to reach deeper by using the depth profiling method or the hardness measurements have to be made closer to the sidewall surface by using lower testing loads. The drawback of depth profiling is that it is destructive.

An interesting fact is that the ore-based steel sample at position $\alpha_{BN} = 135°$ had the least compressive residual stresses measured during the project while the BN value of that position was the highest. This is in accordance with the theory but it can not be clarified here if the BNA is capable to analyse a depth of in this case 100 µm while also being sensitive for residual stress differences in depths of a few micrometres. Therefore, more data have to be acquired and tested for correlation.

6 Summary and Future Work

The project was based on applying different methods on samples taken from one ore-based steel crankshaft and one recycled steel crankshaft. The decision on where to take samples from the crankshafts' sidewall was guided by the corresponding BNA data which served as a measure for grindability. These are the main observations that were repeatedly made during the comparison of the samples:

- The recycled steel bar shows significantly larger pearlite grains than the ore-based steel bar. The pearlite grains in both steels are embedded in a ferrite grain network. The grain size difference is not present in the crankshafts' microstructure. The most likely reason is that it is reduced due to hot-forging and the subsequent normalising process.
- Strong inhomogeneity and banding is observed in all sidewall samples. But the samples from the recycled steel crankshaft always show a more inhomogeneous microstructure with broader, more zoned and contrasted bands. These are most likely indicating chemical composition gradients in the sample that cause different etching.
- The prior austenite grain size is similar when comparing both crankshafts at a given position. Slight differences appear within the different positions in every crankshaft. This is most likely related to different degrees of deformation during forging.
- Despite different prior austenite grain sizes, the martensitic microstructure in the hardened area is not affected and all sidewall samples show similar hardness close to the sidewall surface.
- The hardenability was always higher in the recycled steel samples than in the ore-based samples when defining a deeper reaching hardened area as high hardenability. This indicates that the two investigated steels do not have the same chemical composition.

- The residual stresses in the sidewall are compressive at all investigated positions. Depending on the position they vary relatively much.

To answer the research question, it can be said that the microstructure in the hardened areas is similar for both crankshafts. The microstructure is martensitic and shows to have a similar hardness close to sidewall surface. However, the macroscopic view on the sidewall samples shows a higher degree of inhomogenity, a stronger banding-tendency and a higher hardenability in the recycled samples. When comparing the all samples in terms of Barkhausen noise and residual stresses, which were used as a grindability measure, it does not seem that the differences mentioned above have a strong impact on grindability.

It is imaginable that the testing methods used during the thesis project are not capable of resolving possible differences in the two steels that have a strong impact on grindability. Thus, some suggestions for future work are given in the following:

Regarding the microstructures' inhomogeneity at the sidewalls of the crankshafts made of both steels, it would be of high interest to know how the composition differs from band to band. Energy-dispersive X-ray spectroscopy (EDS) measurements could be performed to get an insight in how the composition varies within the bands in all samples. But not only the composition of the bands should be looked at. The role of different inclusions, their composition, alignment and size has to be considered as well as previous studies have already shown.

Regarding the hardenability difference of both steels, it should be precisely investigated in which manner a compositional difference may affect grindability. Although the hardness close to the sidewall is similar for all samples, regardless of steel batch, different compositions may result in different types and amounts of inclusions. These again can have a direct influence on the grindability. Here reference can be made to the above standing suggestions. The investigations on the crankshafts have to take one step deeper into the material and reveal more detailed information on overall and band composition, inclusions and the effects of these aspects.

As already mentioned, both crankshafts were the first crankshafts being ground after dressing the grinding wheel. It should be investigated how the grindability changes after the grinding of several crankshafts in a row without wheel dressing. The wheel wear rate and its effects could serve as another grindability assessment

method. Here the inclusion properties are expected to play a major role (e.g. protection or blunting of abrasives due to hard inclusions).

The experimental procedure described in this thesis can be a useful manual for further research in this field, especially when an obviously thermally damaged crankshaft is to be analysed. The analysed crankshafts would have most likely passed the inspections when considering the BNA data as a measure and the messages in the log file. Investigations on a thermally damaged crankshaft with grinding burns following the methodology and experiments of this thesis project could probably generate more new knowledge and ideas on why some crankshafts are ground without issues and others not.

Bibliography

[1] M. Doverbo, "Correlation between material properties, grinding effects and Barkhausen noise measurements for two crankshaft steels," Chalmers University of Technology, 2012.

[2] T. J. Machado, "Machinability of Crankshaft Steel: On the Influence of Batch-to-Batch Material Variations Master's thesis in Production Engineering," Chalmers University of Technology, 2019.

[3] H. Berns and W. Theisen, *Ferrous materials: Steel and cast iron*. Springer Berlin Heidelberg, 2008, ISBN: 9783540718475. DOI: 10.1007/978-3-540-71848-2.

[4] F. Klocke, *Manufacturing Processes 2*. Springer Berlin Heidelberg, 2009, ISBN: 978-3-540-92258-2. DOI: 10.1007/978-3-540-92259-9.

[5] H. K. D. H. Bhadeshia and R. Sir Honeycombe, *Steels - Microstructure and Properties*, 3rd ed. Oxford: Butterworth-Heinemann, 2006, ISBN: 0-7506-8084-9.

[6] G. Krauss, *Steels : Processing, Structure, and Performance.* ASM International, 2015, ISBN: 1-62708-083-X.

[7] Krupp Gerlach, *Motor Vehicle Crankshafts: Design, engineering and manufacture*. Landsberg am Lech: Verlag Moderne Industrie, 2001. [Online]. Available: https://books.google.se/books?id=GvTuMAAACAAJ.

[8] H. Kitahara, R. Ueji, N. Tsuji, and Y. Minamino, "Crystallographic features of lath martensite in low-carbon steel," *Acta Materialia*, vol. 54, no. 5, pp. 1279–1288, 2006, ISSN: 13596454. DOI: 10.1016/j.actamat.2005.11.001.

[9] S. Kalpakjian and S. R. Schmid, *Manufacturing Engineering and Technology*, 6th ed. Pearson Education, 2010, ISBN: 9780136081685.

[10] M. Grossmann and E. Bain, *Principles of Heat Treatment*, 5th ed. American Society of Metals, 1964.

[11] C. Siebert, D. Doane, and D. Breen, *The Hardenability of Steels - Concepts, Metallurgical Influences and Industrial Applications*. American Society of Metals, 1977.

[12] W. Ding, L. Zhang, Z. Li, Y. Zhu, H. Su, and J. Xu, "Review on grinding-induced residual stresses in metallic materials," *International Journal of Advanced Manufacturing Technology*, vol. 88, no. 9-12, pp. 2939–2968, 2017, ISSN: 14333015. DOI: 10.1007/s00170-016-8998-1.

[13] P. J. Withers and H. K. D. H. Bhadeshia, "Residual stress. Part 1 – Measurement techniques," *Materials Science and Technology*, vol. 17, no. 4, pp. 355–365, 2001. DOI: 10.1179/026708301101509980.

[14] ——, "Residual stress. Part 2 – Nature and origins," *Materials Science and Technology*, vol. 17, no. 4, pp. 366–375, 2001. DOI: 10.1179/026708301101510087.

[15] I. C. Noyan and J. B. Cohen, "Residual Stresses in Materials," *American Scientist*, vol. 79, no. 2, pp. 142–153, 1991. [Online]. Available: https://www.jstor.org/stable/29774322.

[16] C. K. Gupta, *Chemical Metallurgy: Principles and Practice*. Weinheim: WILEY-VCH, 2003, ISBN: 3527303766.

[17] T. W. Miller, J. Jimenez, A. Sharan, and D. A. Goldstein, *The Making, Shaping and Treating of Steel*, R. J. Fruehan, Ed. 1998, ch. Oxygen Steelmaking Process, ISBN: 0–930767–02–0.

[18] J. A. T. Jones, B. Bowman, and P. A. Lefrank, *The Making, Shaping and Treating of Steel*, R. J. Fruehan, Ed. 1998, ch. Electric Furnace Steelmaking, ISBN: 0–930767–02–0.

[19] A. Ghosh, *Secondary Steelmaking: Principles and Application*. CRC Press, 2001, ISBN: 0849302641.

[20] Stresstech, *Grinding burn detection*. [Online]. Available: https://www.stresstech.com/en/solutions/grinding-burn-detection/.

[21] ——, *Barkhausen Noise Analysis*. [Online]. Available: https://www.stresstech.com/en/knowledge/non-destructieve-testing-methods/barkhausen-noise-analysis/%7B%5C%%7D0A.

[22] R. Tomkowski, Ed., *The Barkhausen Noise Measurements - Good Practice Guide*. KTH Royal Institute of Technology, 2018, ISBN: 978-91-7729-978-3.

[23] ——, *Barkhausen Noise Properties*. [Online]. Available: https://www.stresstech.com/en/knowledge/articles/properties-barkhausen-noise/.

[24] ——, *Barkhausen Noise Analysis*. [Online]. Available: https://www.stresstech.com/en/knowledge/articles/stresstech-bulletin-1-barkhausen-noise-analysis/.

[25] M. E. Fitzpatrick and A. T. Fry, "NPL Good Practice Guide no . 52 : determination of residual stresses by x-ray diffraction Determination of Residual Stresses by X-ray Diffraction - Issue 2," no. 52, 2002.

[26] Stresstech, *Residual stress measurement*. [Online]. Available: `https://www.stresstech.com/en/knowledge/non-destructieve-testing-methods/x-ray-diffraction/`.

[27] *ASTM E112 - 13: Standard Test Methods for Determining Average Grain Size*, ASTM Standard.

[28] T. N. Baker, "Microalloyed steels," *Ironmaking and Steelmaking*, vol. 43, no. 4, pp. 264–307, Apr. 2016. DOI: `10.1179/1743281215Y.0000000063`.

[29] *ASTM E92 - 17: Standard Test Methods for Vickers Hardness and Knoop Hardness of Metallic Materials*, ASTM Standard.

Appendix A – Appendix 1

A.1 Sample Preparation

Table A.1: Grinding and polishing steps and parameters.

Step	Grinding/ polishing surface	Abrasive size	Force per sample	Time	RPM	Rotation direction of disc and sample holder	Comment
1	MD Gekko	#220 paper	30 N	5 min	150/150	same	water
2	MD Allegro	9 µm suspension	30 N	4 min	150/150	same	no water, suspension
3	MD Dac	3 µm suspension	30 N	4 min	150/150	same	no water, suspension
4	MD Nap	1 µm suspension	15 N	1 min	150/150	opposite	no water, suspension